

1 **Polarized Lung Inflammation and Tie2/Angiopoietin-Mediated Endothelial**
2 **Dysfunction during Severe *Orientia tsutsugamushi* Infection**

3

4 **Running title: Pulmonary inflammatory mediators in severe scrub typhus**

5

6 Brandon Trent¹, Yuejin Liang², Yan Xing^{2, #a}, Marisol Esqueda², Yang Wei^{2, #b}, Nam-Hyuk
7 Cho^{3,4}, Hong-Il Kim⁴, Yeon-Sook Kim⁵, Thomas R. Shelite^{2, #c}, Jiyang Cai^{6, #d}, Jiaren Sun^{1,2},
8 Donald H. Bouyer¹, Jinjun Liu^{7,*}, Lynn Soong^{1,2,*}

9

10 ¹Department of Pathology, University of Texas Medical Branch, 301 University Blvd,
11 Galveston, TX 77555-0609

12 ²Department of Microbiology and Immunology, University of Texas Medical Branch, 301
13 University Blvd, Galveston, TX 77555-1070

14 ³Department of Microbiology and Immunology, Seoul National University College of Medicine,
15 Seoul 03080, Republic of Korea

16 ⁴Department of Biomedical Sciences, Seoul National University College of Medicine, Seoul
17 03080, Republic of Korea

18 ⁵Division of Infectious Diseases, Department of Internal Medicine, Chungnam National
19 University School of Medicine, Daejeon 35015, Republic of Korea

20 ⁶Department of Ophthalmology & Visual Sciences, University of Texas Medical Branch,
21 Galveston, 301 University Blvd., Galveston, TX 77555-1106

22 ⁷Department of Physiology and Pathophysiology, School of Basic Medical Sciences, Xi'an
23 Jiaotong University Health Science Center, Xi'an 710061, China

24 #^aCurrent Address: People's Hospital of Henan Province, Henan 450003, China

25 #^bCurrent Address: Core Research Laboratory, The Second Affiliated Hospital of Xi'an Jiaotong

26 University, Xi'an 710004, China

27 #^cCurrent Address: Department of Internal Medicine, Division of Infectious Diseases, University

28 of Texas Medical Branch, 301 University Blvd, Galveston, TX 77555-0435

29 #^dCurrent Address: Department of Physiology, OUHSC, 940 Stanton Young Blvd., Oklahoma

30 City, OK 73104-5042

31

32

33

34 * Corresponding Authors: Jinjun Liu: jupet@163.com; Lynn Soong: lysoong@utmb.edu

35

36

37 **Key Words:** *Orientia tsutsugamushi*, endothelial cell, Tie2, angiopoietin, macrophage

38 **Abstract**

39 *Orientia tsutsugamushi* infection can cause acute lung injury and high mortality in humans;
40 however, the underlying mechanisms are unclear. Here, we tested a hypothesis that dysregulated
41 pulmonary inflammation and Tie2-mediated endothelial malfunction contribute to lung damage.
42 Using a murine model of lethal *O. tsutsugamushi* infection, we demonstrated pathological
43 characteristics of vascular activation and tissue damage: 1) a significant increase of ICAM-1,
44 VEGFR2, and angiopoietin-2 (Ang2) proteins in inflamed tissues and lung-derived endothelial
45 cells (EC), 2) a progressive loss of endothelial quiescent and junction proteins (Ang1, VE-
46 cadherin/CD144, occludin), and 3) a profound impairment of Tie2 receptor at the
47 transcriptional and functional levels. *In vitro* infection of primary human EC cultures and serum
48 Ang2 proteins in scrub typhus patients support our animal studies, implying endothelial
49 dysfunction in severe scrub typhus. Flow cytometric analyses of lung-recovered cells further
50 revealed that pulmonary macrophages (MΦ) were polarized toward an M1-like phenotype
51 (CD80⁺CD64⁺CD11b⁺Ly6G⁻) during the onset of disease and prior to host death, which
52 correlated with the significant loss of CD31⁺CD45⁻ ECs and M2-like
53 (CD206⁺CD64⁺CD11b⁺Ly6G⁻) cells. *In vitro* studies indicated extensive bacterial replication in
54 M2-type, but not M1-type, MΦs, implying the protective and pathogenic roles of M1-skewed
55 responses. This is the first detailed investigation of lung cellular immune responses during acute
56 *O. tsutsugamushi* infection. It uncovers specific biomarkers for vascular dysfunction and M1-
57 skewed inflammatory responses, highlighting future therapeutic research for the control of this
58 neglected tropical disease.

59

60 **Author Summary**

61 Scrub typhus is a life-threatening disease, infecting an estimated one million people yearly.
62 Acute lung injury is the most common clinical observation; however, its pathogenic biomarkers
63 and mechanisms of progression remain unknown. Here, we used a lethal infection mouse model
64 that parallels certain aspects of severe scrub typhus, primary human endothelial cell cultures, and
65 patient sera to define pathogenic biomarkers following *Orientia tsutsugamushi* infections. We
66 found a significant increase in the levels of endothelial activation/stress markers (angiopoietins
67 and ICAM-1) in infected mouse lungs and in patient sera, but a progressive loss of endothelium-
68 specific Tie2 receptor and junction proteins (VE-cadherin), at severe stages of disease. These
69 signs of vasculature disruption positively correlated with the timing and magnitude of
70 recruitment/activation of proinflammatory M Φ subsets in infected lungs. Bacterial growth *in*
71 *vitro* was favored in M2-like, but not in M1-like, M Φ s. This study, for the first time, reveals
72 endothelial malfunction and dysregulated inflammatory responses, suggesting potential
73 therapeutic targets to ameliorate tissue damage and pathogenesis.

74 **Introduction**

75 Scrub typhus is a febrile and potentially lethal illness that infects an estimated one million
76 individuals per year [1]. The disease is caused by infection with the bacterium, *Orientia*
77 *tsutsugamushi*. Nearly a third of the human population lives in endemic areas, known as the
78 “tsutsugamushi triangle”, although recent reports have identified scrub typhus in South America,
79 which was previously believed to be free of scrub typhus [1, 2]. Within endemic areas, scrub
80 typhus is reported to cause a substantial proportion (approximately 15-23%) of reported febrile
81 illness [3, 4]. If left untreated, scrub typhus can manifest as interstitial pneumonia, myocardial
82 and hepatic inflammation, and meningoencephalitis. [5]. Mild interstitial pneumonitis is typically
83 the extent of pulmonary involvement during self-resolving or promptly treated scrub typhus.
84 However, life-threatening pathologies can arise in severe cases, including lung hemorrhage,
85 edema buildup, diffuse alveolar damage, and interstitial cellular infiltration [6]. Acute respiratory
86 distress syndrome and lung damage are associated with high mortality and present in 6.75-25%
87 of scrub typhus patients [5, 7]; however, there is no detailed investigation of the underlying
88 mechanisms responsible for pulmonary endothelial dysfunction and inflammation.

89

90 Being an obligate intracellular bacterium, *O. tsutsugamushi* can infect a variety of host cells but
91 primarily replicate in macrophages (MΦs)[8], dendritic cells [9], and endothelial cells (ECs) [6,
92 8]. The bacteria enter host cells via the phagosome [10] or endosome [11], which they
93 subsequently escape to begin replication in the cytoplasm. Infection-triggered cellular responses,
94 including the activation of activator protein-1 (AP-1) and NF-κB pathways, the production of
95 proinflammatory cytokines (IL-1β, TNF-α, IL-8/CXCL8), and the expression of distinct gene
96 profiles, have been examined *in vitro* by using primary human umbilical vein endothelial cells

97 (HUVEC) [12], human epithelial/EC-like ECV304 cell line [13], human monocytes or MΦs
98 [14]. Prolonged infection can result in EC death via apoptosis [15], but there is limited
99 information on endothelial responses during the course of *O. tsutsugamushi* infection [16].
100 Sublethal *O. tsutsugamushi* infection studies in outbred Swiss CD-1 mice [17], as well as clinical
101 studies of human patients [18], have shown significant elevation of endothelial activation
102 markers (ICAM-1, VCAM-1, E-Selectin, etc.) in the serum of infected individuals; however,
103 endothelium-focused analyses during *in vivo* infection remain largely unexplored. Several
104 studies have characterized the response and activation of MΦs during *O. tsutsugamushi* infection
105 [19, 20]. *In vitro* and *ex vivo* experiments have shown that human monocytes/MΦs in the
106 circulation adopt an inflammatory “M1” type transcriptional profile after *O. tsutsugamushi*
107 infection, although little is known regarding tissue specific macrophages or the presence of
108 alternatively activated “M2”-type macrophages [21].

109
110 The delicate balance of EC quiescence and activation is crucial during systemic infection. While
111 EC activation promotes adherence and recruitment of innate and adaptive immune cells for
112 pathogen clearance, prolonged activation can lead to EC cytotoxicity, impaired barrier function,
113 and host mortality [22]. One of the critical mechanisms to control EC activation status and
114 cellular function is through competitive interactions between angiotensin-1 (Ang1) and Ang2
115 ligands with their receptor, Tie2, a protein tyrosine kinase that is predominately expressed on
116 ECs in humans and mice. Tie2 activation and phosphorylation via binding with Ang1 (produced
117 by pericytes and platelets [23]) promote EC quiescence, which limits leukocyte adhesion and
118 maintains EC survival and vascular barrier integrity [24]. Infection- or inflammation-triggered
119 release of Ang2 (normally stored within the Weibel-Palade bodies in ECs [25, 26]) can compete

120 with Ang1 binding Tie2 to antagonize its function [27]. Inhibition of Tie2 signaling via Ang2
121 binding stimulates leukocyte adhesion, vascular barrier destabilization, and inflammation [28,
122 29]. Thus, Ang2/Ang1 expression ratios and Tie2 activation status are important biomarkers for
123 the pathogenesis of systemic infection, such as severe sepsis and malaria [30, 31].

124

125 To investigate endothelial alterations during severe *O. tsutsugamushi* infection, we have recently
126 developed a lethal intravenous *O. tsutsugamushi* infection model in C57BL/6 mice [32-34],
127 which parallels aspects of severe scrub typhus in humans. In our lethal models, bacterial loads in
128 both the spleen and liver reached peak levels around or shortly after the onset of disease (days 6-
129 8 post-infection), and are reduced significantly by days 10-12. In contrast, lung bacterial loads
130 remain elevated throughout infection [35]. All mice expire by days 12-13, suggesting unknown
131 mechanisms of pathogenesis are at work during late infection [32, 35]. Given that the lungs are a
132 major organ for *O. tsutsugamushi* infection in humans and in different animal models, and that
133 elevated ratios of *ANG2/ANG1* transcripts are pathological hallmarks in lethal infection models
134 [32, 35], we hypothesize that dysregulated pulmonary inflammation and Tie2/Ang2-mediated
135 endothelial dysfunction contribute to disease pathogenesis at late stages of *O. tsutsugamushi*
136 infection.

137

138 In this study, we utilized a lethal infection model in C57BL/6 mice, *in vitro* infection systems
139 (human EC cultures, and bone marrow-derived MΦ subsets), as well as sera from scrub typhus
140 patients to reveal positive correlations between vascular dysfunction, activation of innate
141 immune cells, and disease progression. We focused on two cellular subsets known to be sites of
142 *O. tsutsugamushi* replication, ECs and MΦs, to characterize their activation and polarization *in*

143 *vivo*. To the best of our knowledge, this is the first report to delineate MΦ subsets in inflamed
144 lungs and their positive correlation with Tie2 malfunction during late stages of severe infection.
145

146 **Results**

147

148 **Pulmonary EC activation and tight junction disruption during infection in mice**

149 Given that the lung is a major site of *O. tsutsugamushi* infection in humans and animal models
150 [6, 32] and that EC activation and disruption of vascular barrier integrity are principal steps for
151 acute lung injury in sepsis and pneumonia models [36], we sought to investigate pulmonary EC
152 activation in C57BL/6 mice following i.v. inoculation with a lethal dose of *O.*
153 *tsutsugamushi* Karp ($\sim 1.325 \times 10^6$ viable bacteria in 200 μ l of PBS). Inoculation via this route
154 establishes bacterial replication in the lungs accompanied by interstitial pneumonitis and alveolar
155 thickening (S1A Fig, [35]). Immunofluorescent staining of frozen lung sections revealed
156 increased ICAM-1-positive (green) vascular staining on days 2 (D2) to 9, as well as a close
157 association of bacterial (red) with activated endothelium at D9 (Fig 1A, boxed area, Fig 1C). To
158 examine endothelial structure and adherens junctions, we co-stained lung sections with GSL I-B₄
159 lectin (specific for α -galactose residues known to be enriched on the surface of EC) and anti-VE-
160 cadherin/CD144 (an adherens junction protein, red), as described in our previous report for
161 neuroinflammation [34]. The VE-cadherin staining was intense and homogenous in the control
162 tissues, but markedly reduced in D2 samples; VE-cadherin staining was nearly absent in some
163 foci of D6 and D9 samples (Fig 1B-C), implying the reduction of junction proteins. In
164 conjunction with the endothelial junction proteins, we co-stained the epithelial junction protein,
165 occludin, and GSL I-B₄ lectin. Consistently, we found a progressive loss of occludin staining on
166 the bronchial epithelium during the infection and a near absence of staining in D9 samples (S1B
167 Fig). These data suggest a progressive and severe loss of vascular barrier integrity in the infected
168 lungs, especially at late stages of acute infection prior to host death (D9) [32].

169

170 To support our immunofluorescent results, we prepared single-cell suspensions from mouse lung
171 tissues and used flow cytometry to examine the frequency of recovered CD31⁺CD45⁻ ECs and
172 their surface ICAM-1 expression. We found that compared with the mock controls, infected lung
173 tissues contained a significant increase in the frequencies of ICAM-1⁺CD31⁺CD45⁻ ECs at D6
174 and D9, respectively ($p < 0.001$, $p < 0.01$, Fig 1D), while there were approximately 5-folds
175 reduction in the frequencies of total ECs at D6 and D9 ($p < 0.001$, S1C Fig). We also examined
176 EC expression of vascular endothelial growth factor receptor 2 (VEGFR2), a critical factor
177 controlling vascular permeability and barrier function [37]. Compared with the mock controls,
178 there was an approximately 6-fold increase in the frequencies of VEGFR2⁺CD31⁺CD45⁻ ECs in
179 the lung tissues at D6 and D9 (Fig 1D). These flow cytometry data reinforced the
180 immunofluorescent results, indicating marked endothelial activation and damage at D6 (the onset
181 of disease) and D9 (prior to host demise). To validate these findings in mice, we infected primary
182 HUVEC cultures with different doses of *O. tsutsugamushi* (3 and 10 MOI) and found a dose-
183 dependent increase in *ICAM1* and *IL8/CXCL8* transcripts at 24 h post-infection (S1D Fig).
184 Collectively, these data indicate infection-triggered endothelial stress and activation,
185 accompanied by progressive vascular damage and tight junction disruption during the course of
186 infection.

187

188 **Alterations in the angiopoietin-Tie2 system during *Orientia* infection**

189 Currently, there are no detailed *in vivo* studies to define molecular mechanisms underlying *O.*
190 *tsutsugamushi* infection-associated vascular damage. For other severe and systemic infections
191 caused by bacteria or viruses, alterations in angiopoietin proteins or their functional Tie2

192 receptor is considered as one of the key mechanisms for vascular dysfunction [38, 39] . Given
193 our previous findings of elevated *ANG2/ANG1* mRNA ratios in mice with severe scrub typhus
194 and in *O. tsutsugamushi*-infected HUVECs [33], we speculated that impairment in Tie2 function
195 occurs in severe scrub typhus [16]. To test this hypothesis, we examined Ang1, Ang2, and Tie2
196 protein levels in the lung tissues via immunofluorescent staining (Figs 2-3). While the mock
197 controls contained relatively high levels of Ang1 (green), with relatively low levels of Ang2
198 (red), we found a modest decrease in Ang1-positive staining but a steady increase in Ang2
199 staining, during the course of infection (Fig 2A). These IFA results were quantified,
200 demonstrating the significant decrease of Ang1 and a significant increase of Ang2 expression
201 during *O. tsutsugamushi* infection that correlated with disease progression (Fig 2B). To validate
202 our findings mouse models, we measured scrub typhus patient sera via specific ELISA assays
203 and found a statistically significant increase in circulating Ang2 levels, which correlated with
204 their *O. tsutsugamushi*-specific antibody titers ($p < 0.05$ and $p < 0.01$, comparing IFA titers of
205 1:640 and 1:1280 with the control subjects, Fig 2C). These human data support our findings
206 obtained from mouse tissues, indicating the potential utility of serum Ang2 levels as a molecular
207 biomarker of scrub typhus severity.

208

209 IFA staining of the Ang1/2 receptor, Tie2, revealed clear Tie2 staining in mock infected controls,
210 however, positive Tie2 staining was nearly absent in some foci of D6 and D9 samples (Fig 3A).
211 To validate these findings, we used Western blot analyses of lung tissues and confirmed a
212 striking reduction of phosphorylated Tie2 (pTie2) and total Tie2 levels at both D6 and D9, as
213 compared with either the mock and D2 samples (Fig 3B), implying impairments at the
214 translational and functional levels. The qRT-PCR analyses further validated a statistically

215 significant decrease in *TIE2* mRNA levels in the lungs at D6 and D10 ($p < 0.01$, compared with
216 the mock controls, Fig 3C), implying impairment at the transcriptional level. These data, together
217 with our previous studies [32, 33], indicate that marked Ang2 production, accompanied with
218 severe impairment in the Tie2 functions, are pathogenic mechanisms of severe vascular damage
219 in *O. tsutsugamushi* infection.

220

221 **M1-like responses in the lungs of infected mice**

222 Having documented progressive endothelial damage and alterations in endothelium-specific
223 biomarkers following *O. tsutsugamushi* infection (Figs 1 and 2), we then examined the timing
224 and magnitude of leukocyte recruitment and activation. Although some reports described
225 leukocyte involvement in *O. tsutsugamushi*-infected mouse spleen and brain [34, 40], there are
226 no detailed studies of innate immune responses in infected lungs. Using immunofluorescent
227 staining, we found that CD45⁺ leukocytes and CD3⁺ T cells were accumulated around Ang2-
228 positive foci in the lungs at D6 and D10, and that CD45-Ang2 or CD3-Ang2 co-stained foci
229 were readily detectable at D10 (yellow, S2A Fig). Flow cytometric analyses revealed a 20-fold
230 increase in total numbers of CD4⁺ T cells at D10, but a statistically significant decrease in
231 percentages of these cells at D6 and D10, respectively ($p < 0.0001$, compared with mock
232 controls, S2B Fig). In contrast, there was a 50-fold increase in total numbers and 2.3-fold
233 increase in percentages of CD8⁺ T cells at D10 (S2C Fig). These findings were consistent with
234 the known importance of CD8⁺ T cells during *O. tsutsugamushi* infection in mice [40, 41].

235

236 Monocytes and MΦs are particularly noteworthy leukocytes during *O. tsutsugamushi* infection,
237 as they can act as a target for bacterial replication and a propagator of the inflammatory response

238 [8, 14], possibly playing a role in *O. tsutsugamushi* dissemination from skin lesions [9, 42].
239 While *in vitro* infection predominantly drives human monocytes/MΦs to M1-like transcription
240 programs [9, 42], our current knowledge on *O. tsutsugamushi*-MΦ interactions in the lungs is
241 still limited. Using IFA staining, we observed co-localization of bacteria (green) with IBA-1⁺
242 MΦs (red) in mouse lungs (S3A Fig). To define monocyte/MΦ responses, we applied reported
243 protocols and gating strategies for flow cytometric analysis of mouse lung monocyte/MΦ subsets
244 [43] (Fig 4A). Compared with the mock controls, D6 and D9 samples had 4- to 5-fold increases
245 in the frequency of CD64⁺CD11b⁺Ly6G⁻ alveolar/interstitial monocytes/MΦs, as well as 6- and
246 14-fold increases in total cell numbers, respectively ($p < 0.01$ and $p < 0.001$, Fig 4B). Of note,
247 nearly all (~97%) pulmonary MΦs displayed an M1-like phenotype
248 (CD80⁺CD64⁺CD11b⁺Ly6G⁻, Fig 4C) at D9. In contrast, while the mock and D2 lung samples
249 contained ~3.2% of M2-like (CD206⁺CD64⁺CD11b⁺Ly6G⁻) cells, these cells were barely
250 detectable at D6 or D9 (Fig 4D). These data suggest extensive recruitment and/or activation of
251 M1-like cells, but marked loss and/or suppression of M2-like cells, during the progression of
252 disease. Likewise, lung qRT-PCR assays confirmed a significant up-regulation of M1 markers
253 (*IFN* γ , *FPR2*, *CD38*, and *NOS2*), but not M2 markers (*CD206*, *EGR2*), at D9 (Fig 5A and B).
254 While the *IL10* up-expression was previously reported by our lab and other groups [44], we also
255 detected an increased expression of *ARGINASE1* (Fig 5B), a marker known for M2 polarization
256 and the growth of other intracellular pathogens [45]. Together with data shown in Fig 4, we
257 concluded that at the onset of disease and beyond, *O. tsutsugamushi* infection preferentially
258 stimulated pro-inflammatory innate responses in M1-like monocytes/MΦs, which correlate with
259 the onset of vascular damage (Figs 1-3).

260

261 **MΦ polarization in favor of *Orientia* replication *in vitro***

262 Because we had demonstrated differential monocyte/MΦ responses *in vivo*, we asked how
263 MΦ polarization might influence intracellular growth of the bacteria. We generated bone
264 marrow-derived MΦs from naïve C57BL/6 mice, polarized cells via pretreatment with LPS (100
265 ng/ml) or recombinant IL-4 (rIL-4, 10 ng/ml) for 24 h, infected cells with *O. tsutsugamushi*
266 (MOI 5), and measured bacterial loads at different time points. Flow cytometry and gene profile
267 analyses of primed but uninfected cells confirmed their corresponding polarization to either
268 classically activated M1 or alternatively activated M2 phenotypes (S3B and C Fig), as
269 documented by others [46]. At 48 h post-infection, IL-4-primed M2 cells contained significantly
270 increased loads of bacteria (judged by the copy number of *Orientia* 47-kDa gene) than LPS-
271 primed M1 cells ($p < 0.01$, Fig 6A). At 72 h post-infection, M2 cells contained 10-fold more
272 bacteria than M1 cells (Fig 6A), with extensive accumulation of bacteria (green) within IBA-1-
273 positive MΦs (red, Fig 6B).

274

275 **Discussion**

276 Despite being an important emerging infectious disease, detailed immunological studies of scrub
277 typhus patient samples or *O. tsutsugamushi*-infected animal tissues during the course of disease
278 are scarce. In this study, we focused on ECs and monocytes/MΦs in the lungs of lethally infected
279 mice to examine the activation of these cellular subsets known to be important cellular targets of
280 *O. tsutsugamushi* *in vivo*. Our findings revealed important parameters and cell-specific
281 alterations associated with acute lung injury and pathogenesis. The endothelium in infected lungs
282 presented progressive Tie2 malfunction, increased Ang2 and ICAM-1 expression and pro-
283 inflammatory MΦs at the onset of disease and severe stages of infection. Since lung damage and

284 vascular malfunction are hallmarks of scrub typhus severity in patients [6], a better
285 understanding of pathogenesis associated with acute lung injury is important for disease control
286 and management.

287

288 The molecular characteristics of endothelial alterations during *O. tsutsugamushi* infection *in vivo*
289 have not been explored. The present study provided evidence for the mechanisms underlying
290 pulmonary injury and vascular dysfunction during *O. tsutsugamushi* infection. First, the timing
291 of ICAM-1 and VEGFR2 expression on the surface of lung-derived CD31⁺CD45⁻ ECs was
292 concurrent with the appearance of signs of vascular injury and decrease in cell junction proteins
293 (Fig 1 and S1 Fig). Since ICAM-1 promotes circulating immune cells to bind to the endothelium
294 and extravasate into inflamed tissues [47], increased ICAM-1 surface expression likely
295 contributed to immune cell influx into the infected mouse lungs (Fig 5, S2 Fig). Our observed
296 *ICAM1* and *IL-8/CXCL8* up-regulation in infected human EC cultures (S1C Fig) were consistent
297 with other reported studies of scrub typhus patients [48]. VEGFR2 is known to be the primary
298 receptor for vascular endothelial growth factor (VEGF) in the endothelium, and the
299 VEGF/VEGFR2 axis regulates microvascular permeability via interacting with VE-cadherin and
300 tight junction proteins [49, 50]. In our hands, we consistently detected a marked increase in
301 VEGFR2 on the surface of infected ECs, but a significant reduction of VE-cadherin (adhesion
302 junctions) in the lungs at D6 and D9. While it is unclear whether increased VEGFR2 expression
303 is directly linked to diminished VE-cadherin expression in infected lungs, our data suggest
304 compromised endothelial barrier integrity during severe *O. tsutsugamushi* infection in the lungs.

305

306 Second, a notable reduction of Tie2 proteins was concurrent with significant Ang2 production
307 and/or release at the severe stages of infection (Figs 2-3). To date, there are no reports for Tie2
308 expression levels in scrub typhus patients or animal models, although our group previously
309 showed increased *ANG2/ANG1* transcript ratios in *O. tsutsugamushi*-infected human EC cultures
310 and mouse tissues [32]. Our findings of significant and progressive reduction in Tie2 protein and
311 its mRNA levels, as well as functional pTie2 level, in the lungs of lethally infection mice are
312 important from basic research and clinical points of view. It is known that the Ang1/Tie2 axis is
313 essential for vascular remodeling and endothelial cell stabilization, as either knockout Ang1 or
314 Tie2 in mice is embryonic lethal [51, 52]. Given the critical function of Tie2 receptor in vascular
315 physiology and integrity, it will be important to further examine whether our observed reduction
316 in Ang1 and Tie2 is due to direct endothelial damage or signaling from nearby pericytes and
317 recruited immune cells. Research in these areas would be of great value, as angiopoietin- or
318 Tie2-targeted therapies have been evaluated as alternative treatment strategies for severe sepsis
319 [53, 54], severe dengue [55], and in cerebral malaria [38] infection models to restore endothelial
320 quiescence during infection. Our clinical observation that increased serum Ang2 in human scrub
321 typhus patients correlates with *O. tsutsugamushi*-specific antibody titers demonstrates the utility
322 of Ang2 as a pathogenic biomarker, and highlights the potential of use Ang2- or Tie2-targeted
323 therapies for severe scrub typhus, as in patients with severe sepsis [29, 30] and malaria [56].

324

325 Monocytes/MΦs play important roles in infection with *O. tsutsugamushi* and other closely
326 related *Rickettsia* species [19, 57]. Previous findings [19] are consistent with our observation of
327 an increased accumulation of CD11b⁺Ly6G⁻ MΦs/monocytes and the close association of IBA-1⁺
328 phagocytes with *Orientia* in the lungs at D6 and D9. Yet, our findings of selective

329 recruitment/expansion of M1-skewed MΦs/monocytes, and the suppression of M2 cell
330 activation, in the infected mouse lungs were particularly novel and important. This is the first *in*
331 *vivo* evidence for M1-polarized MΦ responses in *O. tsutsugamushi*-infected mouse lungs, which
332 was consistent with previous *in vitro* and *ex vivo* studies for M1-skewed gene transcription
333 programs in *O. tsutsugamushi*-infected human monocytes and MΦs [21, 42]. At present, it is still
334 unclear whether the predominately M1 MΦ population we observed contributes to the killing of
335 *O. tsutsugamushi* and the damage of vascular tissues, as seen for protective versus pathogenic
336 roles in other lung infection models [58]. Given the reports that anti-Ang2 antibody treatment
337 during pulmonary bacterial infection can decrease MΦ recruitment and inflammation [26], and
338 that signaling via Tie2 on monocytes/MΦs can promote a proinflammatory profile [59], it will be
339 interesting to determine how Ang2/Ang1 signaling on both endothelial cells and MΦs promote
340 cellular recruitment and activation during *O. tsutsugamushi* infection.

341
342 Conditions that promote the killing or growth of *O. tsutsugamushi* remain unclear, in part due to
343 difficulties in bacterial cultivation, genetic modification, or visualization for studying the host-
344 bacterium interactions [60]. Currently, there are no available reports or data for the phenotype of
345 *Orientia*-carrying MΦ subsets or the roles of arginase-1 *in vivo*. Our *in vitro* comparative studies
346 revealed limited bacterial replication in LPS-primed M1-like MΦs (Fig 6), supporting a previous
347 report for the role of NOS2-mediated mechanisms in the control of *O. tsutsugamushi* Karp strain
348 [19]. Yet, our *in vitro* findings were contradictory to another reported study, in which NO-
349 enhanced the growth of *O. tsutsugamushi* Ikeda bacteria was observed in LPS-activated RAW
350 264.7 murine macrophages at days 6 to 8 post-infection [20]. While the use of different bacterial
351 strains, MΦ sources, and examination times may account for these discrepancies, our study calls

352 for careful examination of the intracellular niche for the replication of these obligate intracellular
353 bacteria under different or physiological conditions. For bone marrow-derived MΦs, we found
354 comparable bacterial loads in LPS- and IL-4-primed cells at 3 h, implying similar attachment and
355 invasion of the bacteria under these two treatments. However, IL-4-primed M2 cells contained
356 10-fold more *O. tsutsugamushi* than LPS-primed M1 cells at 72 h. At present, our data did not
357 exclude the possibility of bacterial growth in LPS-primed M1 cells after prolonged time *in vitro*,
358 or in M1- vs. M2-like MΦs in mouse lungs or other organs. Given the recent report that specific
359 MΦ responses, such as miR-155 and IL-10 production, correlate with prevention of cytokine
360 storm in severe *O. tsutsugamushi* infection [61], it will be important to further examine whether
361 the strong type-1 inflammatory responses *in vivo* [32] and M1-skewed responses (Fig 5) are
362 responsible for marked decrease in M2 MΦs in the lungs. The use of transgenic mouse strains
363 for tracking MΦ subsets would also help reveal whether *O. tsutsugamushi* bacteria preferentially
364 replicate within M2 MΦs *in vitro* or contribute to the impairment of type 2 immune responses.

365

366 While the mouse model used here allows us to examine host-bacterium interactions and immune
367 alterations, this model has some intrinsic limitations, as it bypasses bacterial dissemination from
368 the local/skin sites. Nevertheless, this model has several advantages over self-limited infection
369 models following the subcutaneous or intradermal inoculation of the bacteria via needles into
370 inbred strains of mice [19, 62], for the examination of innate immune responses in visceral
371 organs. Compared to a lethal infection initiated by feeding *O. tsutsugamushi*-infected mites on
372 outbred mice, a technically challenging model with high variability [63], our model provides
373 more consistent results and lethality, permitting the analysis of a given host molecule using gene-
374 targeted knockouts on the C57BL/6 background. More importantly, our lethal model mimics

375 certain pathological aspects of severe scrub typhus observed in humans, uncovering tissue-
376 specific immune alterations that have never been described previously. For example, our findings
377 of elevated Ang2 proteins in *O. tsutsugamushi*-infected lungs and increased *ANG2* expression in
378 multiple organs [32] are consistent with clinical studies of scrub typhus patients (Fig 2), which
379 supports the potential for monitoring serum Ang2 levels as an indicator of disease severity and
380 treatment outcome.

381

382 In summary, this study has revealed new insights into immune dysregulation and pathogenesis of
383 severe scrub typhus. Through comprehensive analyses of *O. tsutsugamushi*-infected mouse lung
384 tissues, we have provided the first evidence for the production of endothelial destabilizing factors
385 and *in vivo* polarization of lung recruited MΦs. Our findings of polarized M1-like responses in
386 the lungs at late stages of disease argue for immune-based restriction of bacterial replication as
387 well as immunopathogenesis. While the molecular mechanisms underlying host-bacterium
388 interaction and immune dysregulation remains unclear at this stage, it is conceivable that serum
389 and tissue Ang2 levels would be a molecular biomarker for severe scrub typhus and a potential
390 therapeutic target for treatment. A better understanding of infection- versus immune-mediated
391 dysregulation will help design treatment strategies for severe scrub typhus cases.

392

393

394

395

396

397

398 **Materials and Methods**

399

400 **Mouse infection and ethics statement**

401 Female C57BL/6 mice were purchased from Envigo (Huntingdon, United Kingdom), maintained
402 under specific pathogen-free conditions and used at 6-9 weeks of age, following protocols
403 approved by the Institutional Animal Care and Use Committee (protocols # 9007082B and
404 1302003) at the University of Texas Medical Branch (UTMB) in Galveston, TX. All mouse
405 infection studies were performed in the ABSL3 facility in the Galveston National Laboratory
406 located at UTMB; all tissue processing and analysis procedures were performed in the BSL3 or
407 BSL2 facilities. All procedures were approved by the Institutional Biosafety Committee, in
408 accordance with Guidelines for Biosafety in Microbiological and Biomedical Laboratories.
409 UTMB operates to comply with the USDA Animal Welfare Act (Public Law 89-544), the Health
410 Research Extension Act of 1985 (Public Law 99-158), the Public Health Service Policy on
411 Humane Care and Use of Laboratory Animals, and the NAS Guide for the Care and Use of
412 Laboratory Animals (ISBN-13). UTMB is a registered Research Facility under the Animal
413 Welfare Act, and has a current assurance on file with the Office of Laboratory Animal Welfare,
414 in compliance with NIH Policy.

415

416 *O. tsutsugamushi* Karp strain was used herein; all infection studies were performed with the
417 same bacterial stocks prepared from Vero cell infection, for which infectious organisms were
418 quantified via a qPCR viability assay [35, 64]. Mice were inoculated intravenously (i.v.)
419 with $\sim 1.325 \times 10^6$ viable bacteria (a lethal dose, 200 μ l) or PBS and monitored daily for weight

420 loss and signs of disease. In most cases, tissue samples (4-5 mice/group) were collected at 2, 6,
421 and 9 (or 10) days post-infection and inactivated for immediate or subsequent analyses.

422

423 Ethical approval for human samples used in this work was granted by the Institutional Review
424 Board of both Seoul National University Hospital (IRB NO 1603-136-751) and Chungnam
425 National University Hospital (IRB NO 2014-12-006). All patients and healthy volunteers
426 provided written informed consent prior to sample collection.

427

428 **Immunofluorescence microscopy and quantification**

429 Mouse lung tissues were processed for immunofluorescent staining, as in our previous report
430 [34]. Briefly, 6- μ m frozen sections were blocked and incubated with the following rat or rabbit
431 anti-mouse antibodies (1:200, purchased from Abcam, Cambridge, MA, USA, unless specified):
432 anti-ICAM1, anti-Ang1, anti-Ang2 (R&D Systems/Biotechne, McKinley Place NE, Minnesota),
433 anti-Tie2, anti-VE-cadherin (adherence junctions), anti-occludin (epithelial tight junctions), anti-
434 IBA-1 (ionised calcium binding adapter molecule-1, a M Φ marker), anti-CD45 (BD Bioscience,
435 San Jose, CA, USA), or anti-Ang2 (R&D Systems). Staining endothelium in sections was done
436 with FITC-conjugated *Griffonia Simplicifolia* lectin I (1:100, GSL I-B₄ lectin, Vector Lab,
437 Burlingame, CA, USA). Bacteria was stained in various sections using rabbit anti-*O.*
438 *tsutsugamushi* Karp serum (1:500) [35]. Bound antibodies were visualized by using Alexa Fluor
439 488- or 555-conjugated, goat anti-rat or anti-rabbit IgG (H+L, 1:1,000-1:2,000, Life
440 Technologies, Grand Island, NY, USA). All sections were stained with DAPI (1:5,000, Sigma-
441 Aldrich, St. Louis, MO, USA). Infected sections stained with secondary Abs and DAPI only
442 served as negative controls to optimize staining conditions. For each section, at least 6 low- and

443 6 high-magnification fields of the lung sections were imaged on a Carl Zeiss Axio Observer
444 fluorescence microscope (Carl Zeiss Microscopy LLC, Thornwood, NY, USA) equipped with
445 ApoTome and Zen imaging software. Acquisition settings were identical among samples of
446 different experimental groups. Representative images at each time point are presented. To
447 measure fluorescent intensity of given markers, gray levels across the entire tissue image (low-
448 magnification, 4 independent images per group) were measured via ImageJ under the same
449 parameter setting. Data are presented at mean \pm SEM of the group.

450

451 For *in vitro* studies, cells were seeded onto coverslips in 24-well plates (Falcon Corning,
452 Corning, NY, USA). At indicated times of infection, slides were washed, fixed with 4% PFA for
453 20 min, and permeabilized with Triton X-100 for 15 min. After blocking with 10% BSA/3%
454 goat serum for 1 h, cells were incubated with serum collected from *Orientia*-infected mice
455 (1:1,500) or rabbit anti-IBA-1 (1:250, Abcam) (1:50) at 4°C overnight and then with a secondary
456 Ab: goat anti-mouse Alexa Fluor 488 (Thermo Fisher Scientific, Waltham, MA, USA) or donkey
457 anti-rabbit Alexa Fluor 594 (Invitrogen/Thermo Fisher Scientific) and DAPI (1:1000, Thermo
458 Fisher Scientific). The cover slips were mounted on slides by using an Antifade Mountant
459 solution (Invitrogen/Thermo Fisher Scientific). Images were taken using an Olympus IX51
460 microscope (Olympus Corporation, Tokyo, Japan).

461

462 **Flow cytometry**

463 Equivalent portions of lung tissues were harvested from infected and control mice, minced, and
464 digested with 0.05% collagenase type IV (Gibco/Thermo Fisher Scientific) in Dulbecco's
465 Modified Eagle's Medium (DMEM, Sigma-Aldrich, St. Louis, MO) for 30 mins at 37°C.

466 Minced tissues were loaded into Medicons and homogenized using a BD Mediamachine System
467 (BD Biosciences, Franklin Lakes, NJ). Lung single-cell suspensions were made by passing lung
468 homogenates through 70- μ m cell strainers. Spleen homogenates were made by passing tissue
469 through a 70- μ m strainer. Lymphocytes were enriched by using Lympholyte-M Cell Separation
470 Media (Burlington, NC). Red blood cells were removed by using Red Cell Lysis Buffer (Sigma-
471 Aldrich). Leukocytes were stained with the Fixable Viability Dye (eFluor 506)
472 (eBioscience/Thermo Fisher Scientific, Waltham, MA) for live/dead cell staining, blocked with
473 Fc γ R blocker, and stained with fluorochrome-labeled antibodies (Abs). The following Abs
474 purchased from Thermo Fisher Scientific and BioLegend (San Diego CA): PE-Cy7-anti-CD3 ϵ
475 (145-2C11), Pacific Blue-anti-CD4 (GK1.5), APC-Cy7-anti-CD8a (53-6.7), APC-anti-Ly6G
476 (1A8-Ly6G), APC-anti-CD31 (390), PE-anti-VEGFR2 (Avas12a1), FITC-anti-ICAM-1
477 (YN1/1.7.4), Pacific Blue-anti-CD45 (30-F11), PE-anti-CD80 (16-10A1), BV421-anti-CD206
478 (CO68C2), FITC-anti-CD64 (X54-5/7.1), PerCP-Cy5.5-anti-CD11b (M1/70). Cells were fixed in
479 2% paraformaldehyde overnight at 4°C before cell analysis. Data were collected by a BD
480 LSRFortessa (Becton Dickinson, San Jose, CA) and analyzed using FlowJo software version
481 8.86 (Tree Star, Ashland, OR). As previously reported for mouse lung tissues [65] CD45⁺CD31⁻
482 and CD45⁻CD31⁺ cells were considered hematopoietic cells and endothelial cells by flow
483 cytometry, respectively.

484

485 **Western blot**

486 Protein from lung tissues was extracted with a RIPA lysis buffer (Cell Signaling Technology,
487 Danvers, MA) and quantified with BCA Protein Assay kit (Thermo Fisher Scientific). Protein
488 samples (40 μ g/lane) were loaded onto 4-20% SDS-PAGE gels (Bio-Rad Laboratories, Hercules,

489 CA, USA) and transferred onto nitrocellulose membranes (Bio-Rad Laboratories). After
490 blocking non-specific binding sites, membranes were respectively incubated with rabbit Abs
491 specific to mouse Tie2 (1:500, Abcam), phospho-Tie2 (1:400, R&D System, USA), and β -actin
492 (1:15000, Novus Biologicals, USA), and an anti-rabbit secondary antibody (SouthernBiotech,
493 Birmingham, AL, USA). After treatment with the Maximum Sensitivity Substrate (Thermo
494 Fisher Scientific) for 1 min, the light signals were captured by Luminescent Image Analyzer
495 (ImageQuant LAS 4000, GE Healthcare Bio-Sciences AB, Sweden). Protein bands were
496 quantified by using image analysis software (ImageJ). Three independent experiments were
497 performed.

498

499

500 **Infection of mouse bone marrow-derived M Φ s**

501 Bone marrow cells were collected from mouse femur and tibia and treated with a red cell lysis
502 buffer (Sigma). For M Φ generation, bone marrow cells were grown in DMEM (Gibco) with 10%
503 FBS, penicillin/streptomycin antibiotics, and 40 ng/ml M-CSF (BioLegend) and incubated at
504 37°C. Media was changed at day 3, and cells were collected at day 7 and seeded onto 6- or 24-
505 well plates for overnight. M Φ s were treated with either 100 ng/ml LPS (for M1 polarization) or
506 10 ng/ml mouse rIL-4 (for M2 polarization, Peprotech, Rocky Hill, NJ) for 24 h. Cells were then
507 infected with *O. tsutsugamushi* (5 MOI) and centrifuged at 2,000 RPM for 5 min to synchronize
508 infection of the cells.

509

510 **Quantitative PCR and reverse transcriptase PCR (qPCR and qRT-PCR)**

511 To determine bacterial loads, bone marrow-derived MΦs were collected at 3, 24, 48, and 72 hpi
512 by using a DNeasy kit (Qiagen) and used for qPCR assays, as previously described [32].
513 Bacterial loads were normalized to total nanogram (ng) of DNA per μL for the same sample, and
514 data are expressed as the gene copy number of 47-kDa protein per picogram (pg) of DNA. The
515 copy number for the 47-kDa gene was determined by known concentrations of a control plasmid
516 containing single-copy insert of the gene. Gene copy numbers were determined via serial dilution
517 (10-fold) of the control plasmid.

518

519 To measure host gene expression, mouse tissues or *in vitro*-infected cells were respectively
520 collected in RNALater (Ambion, Austin, TX) or Trizol solution at 4°C overnight to inactivate
521 infectious bacteria and stored at -80°C for subsequent analyses. Total RNA was extracted by
522 using RNeasy mini kits (Qiagen) and digested with RNase-free DNase (Qiagen); cDNA was
523 synthesized with the iScript cDNA synthesis kit (Bio-Rad Laboratories, Hercules, CA). The
524 quantitative RT-PCR (qRT-PCR) assays were performed with iTaq SYBR Green Supermix and a
525 CFX96 Touch Real-Time PCR Detection System (Bio-Rad). PCR assays were denatured for 3
526 min at 95°C, followed by 40 cycles of 10s at 95°C and 30s at 60°C. Melt-curve analysis was also
527 used to check the specificity of the amplification reaction. Relative abundance of transcripts was
528 calculated by using the $2^{-\Delta\Delta\text{CT}}$ method and compared to housekeeping genes glyceraldehyde-3-
529 phosphate dehydrogenase (GAPDH) or β -actin. Primers used in these analyses are listed in Table
530 S1.

531

532 **Human umbilical vein endothelial cell (HUVEC) infection**

533 HUVECs (Cell Application, San Diego, CA) were maintained in complete Prigrow I medium
534 supplemented with 3% heat-inactivated FBS (Applied Biological Materials, Vancouver, Canada)
535 in 5% CO₂ at 37°C. All *in vitro* experiments were performed between cell passages 5 and 7, as
536 described previously [33, 66]. For infection, HUVECs were cultivated in Prigrow I medium with
537 10% FBS and seeded onto 6-well plates (Corning Inc., Corning, NY). Confluent monolayers
538 were infected with *Orientia* (3 and 10 MOI) for 24 h and compared with uninfected controls.

539

540 **Human serum collection and measurement of Ang2 by ELISA**

541 Human serum samples were collected from healthy volunteers ($n = 8$) and scrub typhus patients
542 ($n = 32$) after obtaining informed consent at the Chungnam National University Hospital in
543 Daejeon, South Korea. Scrub typhus diagnosis was confirmed based on clinical symptoms and a
544 positive serology: a 4-fold or greater rise in the titer of paired plasma or single cut-off titer of an
545 IgM antibody $\geq 1:160$ by an indirect immunofluorescence antibody assay (IFA) against *O.*
546 *tsutsugamushi* antigens or passive hemagglutination assay (PHA) during hospital admission.
547 Healthy volunteers had never been previously diagnosed with scrub typhus, and their sera were
548 negative when examined by IFA. Patient plasma samples were classified into four groups based
549 on their IFA titers. Ang2 concentration was determined by using a commercial ELISA kit
550 (Abcam), according to manufacturer's instructions.

551

552 **Human antibody titer measured by IFA**

553 L929 cells infected with three strains of *O. tsutsugamushi* (Boryong, Karp, and Gilliam strains)
554 were harvested, mixed in equal amounts, and used as antigens to measure total IgG titers against
555 *O. tsutsugamushi* via IFA. Briefly, infected L929 cells were harvested, washed with PBS, seeded

556 onto Teflon-coated spot slides, and fixed with cold acetone for 10 min. The slides were stored at
557 -70°C until use. Two-fold serially diluted (1:40 to 1:1280 in PBS) patient sera was added to the
558 antigen-coated spot on the slide and incubated for 30 min in a wet chamber at room temperature.
559 An Alexa Fluor 488-conjugated goat anti-human IgG (diluted 1:1000 in PBS, Molecular Probes,
560 Waltham, MA, USA) was used as the secondary antibody. The stained slides were examined
561 under an Olympus FV1000 laser scanning confocal microscope (Olympus, Tokyo, Japan). The
562 endpoint titer of IFA was defined as the highest titer showing a fluorescence signal above the
563 background.

564

565 **Statistical analysis**

566 Data were presented as mean \pm standard errors of the mean (SEM). Differences between
567 individual treatment and control groups were determined by using Student's t test, utilizing
568 Welch's correction when appropriate. One-way ANOVA was used for multiple group
569 comparisons with a Tukey's Post Hoc for comparisons between groups. Statistically significant
570 values are referred to as *, $p < 0.05$; **, $p < 0.01$; ***, $p < 0.001$; and ****, $p < 0.0001$.

571

572 **Acknowledgements**

573 The authors thank Dr. David Walker for generously providing BSL-3 laboratory equipment and
574 space for conducting experiments, Nicole Mendell for continued training and technical help in
575 many aspects of this study, Dr. Juan Olano and the UTMB Immunology Joint Lab Group for
576 providing helpful suggestions, and Dr. Sherry Haller for manuscript editing assistance.

577

578

579 **References**

- 580 1. Paris DH, Shelite TR, Day NP, Walker DH. Unresolved problems related to scrub
581 typhus: a seriously neglected life-threatening disease. *Am J Trop Med Hyg.* 2013;89(2):301-7.
582 doi: 10.4269/ajtmh.13-0064. PubMed PMID: 23926142; PubMed Central PMCID:
583 PMCPMC3741252.
- 584 2. Kim G, Ha NY, Min CK, Kim HI, Yen NT, Lee KH, et al. Diversification of *Orientia*
585 *tsutsugamushi* genotypes by intragenic recombination and their potential expansion in endemic
586 areas. *PLoS Negl Trop Dis.* 2017;11(3):e0005408. Epub 2017/03/01. doi:
587 10.1371/journal.pntd.0005408. PubMed PMID: 28248956; PubMed Central PMCID:
588 PMCPMC5348041.
- 589 3. Brown GW, Robinson DM, Huxsoll DL, Ng TS, Lim KJ. Scrub typhus: a common cause
590 of illness in indigenous populations. *Trans R Soc Trop Med Hyg.* 1976;70(5-6):444-8. PubMed
591 PMID: 402722.
- 592 4. Phongmany S, Rolain JM, Phetsouvanh R, Blacksell SD, Soukkhaseum V, Rasachack B,
593 et al. Rickettsial infections and fever, Vientiane, Laos. *Emerg Infect Dis.* 2006;12(2):256-62. doi:
594 10.3201/eid1202.050900. PubMed PMID: 16494751; PubMed Central PMCID:
595 PMCPMC3373100.
- 596 5. Varghese GM, Janardhanan J, Trowbridge P, Peter JV, Prakash JA, Sathyendra S, et al.
597 Scrub typhus in South India: clinical and laboratory manifestations, genetic variability, and
598 outcome. *Int J Infect Dis.* 2013;17(11):e981-7. Epub 2013/07/26. doi:
599 10.1016/j.ijid.2013.05.017. PubMed PMID: 23891643.
- 600 6. Hsu YH, Chen HI. Pulmonary pathology in patients associated with scrub typhus.
601 *Pathology.* 2008;40(3):268-71. doi: 10.1080/00313020801911488. PubMed PMID: 18428046.

- 602 7. Wang CC, Liu SF, Liu JW, Chung YH, Su MC, Lin MC. Acute respiratory distress
603 syndrome in scrub typhus. *Am J Trop Med Hyg.* 2007;76(6):1148-52. PubMed PMID:
604 17556627.
- 605 8. Moron CG, Popov VL, Feng HM, Wear D, Walker DH. Identification of the target cells
606 of *Orientia tsutsugamushi* in human cases of scrub typhus. *Mod Pathol.* 2001;14(8):752-9. doi:
607 10.1038/modpathol.3880385. PubMed PMID: 11504834.
- 608 9. Paris DH, Phetsouvanh R, Tanganuchitcharnchai A, Jones M, Jenjaroen K, Vongsouvath
609 M, et al. *Orientia tsutsugamushi* in human scrub typhus eschars shows tropism for dendritic cells
610 and monocytes rather than endothelium. *PLoS Negl Trop Dis.* 2012;6(1):e1466. Epub
611 2012/01/10. doi: 10.1371/journal.pntd.0001466. PubMed PMID: 22253938; PubMed Central
612 PMCID: PMCPMC3254662.
- 613 10. Koo JE, Hong HJ, Dearth A, Kobayashi KS, Koh YS. Intracellular invasion of *Orientia*
614 *tsutsugamushi* activates inflammasome in asc-dependent manner. *PLoS One.* 2012;7(6):e39042.
615 Epub 2012/06/18. doi: 10.1371/journal.pone.0039042. PubMed PMID: 22723924; PubMed
616 Central PMCID: PMCPMC3377614.
- 617 11. Chu H, Lee JH, Han SH, Kim SY, Cho NH, Kim IS, et al. Exploitation of the endocytic
618 pathway by *Orientia tsutsugamushi* in nonprofessional phagocytes. *Infect Immun.*
619 2006;74(7):4246-53. doi: 10.1128/IAI.01620-05. PubMed PMID: 16790799; PubMed Central
620 PMCID: PMCPMC1489698.
- 621 12. Cho NH, Seong SY, Huh MS, Kim NH, Choi MS, Kim IS. Induction of the gene
622 encoding macrophage chemoattractant protein 1 by *Orientia tsutsugamushi* in human endothelial
623 cells involves activation of transcription factor activator protein 1. *Infect Immun.*
624 2002;70(9):4841-50. PubMed PMID: 12183528; PubMed Central PMCID: PMCPMC128290.

- 625 13. Cho KA, Jun YH, Suh JW, Kang JS, Choi HJ, Woo SY. *Orientia tsutsugamushi* induced
626 endothelial cell activation via the NOD1-IL-32 pathway. *Microb Pathog.* 2010;49(3):95-104.
627 Epub 2010/05/12. doi: 10.1016/j.micpath.2010.05.001. PubMed PMID: 20470879.
- 628 14. Cho NH, Seong SY, Huh MS, Han TH, Koh YS, Choi MS, et al. Expression of
629 chemokine genes in murine macrophages infected with *Orientia tsutsugamushi*. *Infect Immun.*
630 2000;68(2):594-602. PubMed PMID: 10639422; PubMed Central PMCID: PMCPMC97181.
- 631 15. Kim MK, Kee SH, Cho KA, Chung MH, Lim BU, Chang WH, et al. Apoptosis of
632 endothelial cell line ECV304 persistently infected with *Orientia tsutsugamushi*. *Microbiol*
633 *Immunol.* 1999;43(8):751-7. PubMed PMID: 10524792.
- 634 16. Soong L. Dysregulated Th1 Immune and Vascular Responses in Scrub Typhus
635 Pathogenesis. *J Immunol.* 2018;200(4):1233-40. doi: 10.4049/jimmunol.1701219. PubMed
636 PMID: 29431689; PubMed Central PMCID: PMCPMC5812358.
- 637 17. Sunyakumthorn P, Paris DH, Chan TC, Jones M, Luce-Fedrow A, Chattopadhyay S, et
638 al. An intradermal inoculation model of scrub typhus in Swiss CD-1 mice demonstrates more
639 rapid dissemination of virulent strains of *Orientia tsutsugamushi*. *PLoS One.* 2013;8(1):e54570.
640 Epub 2013/01/16. doi: 10.1371/journal.pone.0054570. PubMed PMID: 23342173; PubMed
641 Central PMCID: PMCPMC3546997.
- 642 18. Otterdal K, Janardhanan J, Astrup E, Ueland T, Prakash JA, Lekva T, et al. Increased
643 endothelial and macrophage markers are associated with disease severity and mortality in scrub
644 typhus. *J Infect.* 2014;69(5):462-9. Epub 2014/07/01. doi: 10.1016/j.jinf.2014.06.018. PubMed
645 PMID: 24995849.
- 646 19. Keller CA, Hauptmann M, Kolbaum J, Gharaibeh M, Neumann M, Glatzel M, et al.
647 Dissemination of *Orientia tsutsugamushi* and inflammatory responses in a murine model of scrub

- 648 typhus. PLoS Negl Trop Dis. 2014;8(8):e3064. Epub 2014/08/14. doi:
649 10.1371/journal.pntd.0003064. PubMed PMID: 25122501; PubMed Central PMCID:
650 PMC4133189.
- 651 20. Ogawa M, Satoh M, Kataoka M, Ando S, Saijo M. Nitric oxide enhanced the growth of
652 an obligated intracellular bacterium *Orientia tsutsugamushi* in murine macrophages. *Microb*
653 *Pathog.* 2017;107:335-40. Epub 2017/04/12. doi: 10.1016/j.micpath.2017.04.012. PubMed
654 PMID: 28412201.
- 655 21. Tantibhedhyangkul W, Ben Amara A, Textoris J, Gorvel L, Ghigo E, Capo C, et al.
656 *Orientia tsutsugamushi*, the causative agent of scrub typhus, induces an inflammatory program in
657 human macrophages. *Microb Pathog.* 2013;55:55-63. Epub 2012/10/23. doi:
658 10.1016/j.micpath.2012.10.001. PubMed PMID: 23088884.
- 659 22. Grommes J, Soehnlein O. Contribution of neutrophils to acute lung injury. *Mol Med.*
660 2011;17(3-4):293-307. doi: 10.2119/molmed.2010.00138. PubMed PMID: 21046059; PubMed
661 Central PMCID: PMC3060975.
- 662 23. Milam KE, Parikh SM. The angiotensin-Tie2 signaling axis in the vascular leakage of
663 systemic inflammation. *Tissue Barriers.* 2015;3(1-2):e957508. Epub 2015/04/03. doi:
664 10.4161/21688362.2014.957508. PubMed PMID: 25838975; PubMed Central PMCID:
665 PMC4372013.
- 666 24. Thurston G, Rudge JS, Ioffe E, Zhou H, Ross L, Croll SD, et al. Angiotensin-1 protects
667 the adult vasculature against plasma leakage. *Nat Med.* 2000;6(4):460-3. doi: 10.1038/74725.
668 PubMed PMID: 10742156.
- 669 25. Fiedler U, Scharpfenecker M, Koidl S, Hegen A, Grunow V, Schmidt JM, et al. The Tie-
670 2 ligand angiotensin-2 is stored in and rapidly released upon stimulation from endothelial cell

- 671 Weibel-Palade bodies. *Blood*. 2004;103(11):4150-6. Epub 2004/02/19. doi: 10.1182/blood-2003-
672 10-3685. PubMed PMID: 14976056.
- 673 26. Tabruyn SP, Colton K, Morisada T, Fuxe J, Wiegand SJ, Thurston G, et al. Angiopoietin-
674 2-driven vascular remodeling in airway inflammation. *Am J Pathol*. 2010;177(6):3233-43. Epub
675 2010/10/15. doi: 10.2353/ajpath.2010.100059. PubMed PMID: 20952594; PubMed Central
676 PMCID: PMCPMC2993300.
- 677 27. Maisonpierre PC, Suri C, Jones PF, Bartunkova S, Wiegand SJ, Radziejewski C, et al.
678 Angiopoietin-2, a natural antagonist for Tie2 that disrupts in vivo angiogenesis. *Science*.
679 1997;277(5322):55-60. PubMed PMID: 9204896.
- 680 28. Fiedler U, Reiss Y, Scharpfenecker M, Grunow V, Koidl S, Thurston G, et al.
681 Angiopoietin-2 sensitizes endothelial cells to TNF-alpha and has a crucial role in the induction of
682 inflammation. *Nat Med*. 2006;12(2):235-9. Epub 2006/02/05. doi: 10.1038/nm1351. PubMed
683 PMID: 16462802.
- 684 29. Parikh SM, Mammoto T, Schultz A, Yuan HT, Christiani D, Karumanchi SA, et al.
685 Excess circulating angiopoietin-2 may contribute to pulmonary vascular leak in sepsis in
686 humans. *PLoS Med*. 2006;3(3):e46. doi: 10.1371/journal.pmed.0030046. PubMed PMID:
687 16417407; PubMed Central PMCID: PMCPMC1334221.
- 688 30. Orfanos SE, Kotanidou A, Glynos C, Athanasiou C, Tsigkos S, Dimopoulou I, et al.
689 Angiopoietin-2 is increased in severe sepsis: correlation with inflammatory mediators. *Crit Care*
690 *Med*. 2007;35(1):199-206. doi: 10.1097/01.CCM.0000251640.77679.D7. PubMed PMID:
691 17110873.
- 692 31. Petersen JE, Mkumbaye SI, Vaaben AV, Manjurano A, Lyimo E, Kavishe RA, et al.
693 Plasma Ang2 and ADAM17 levels are elevated during clinical malaria; Ang2 level correlates

- 694 with severity and expression of EPCR-binding PfEMP1. *Sci Rep.* 2016;6:35950. Epub
695 2016/10/27. doi: 10.1038/srep35950. PubMed PMID: 27784899; PubMed Central PMCID:
696 PMCPMC5082358.
- 697 32. Soong L, Wang H, Shelite TR, Liang Y, Mendell NL, Sun J, et al. Strong type 1, but
698 impaired type 2, immune responses contribute to *Orientia tsutsugamushi*-induced pathology in
699 mice. *PLoS Negl Trop Dis.* 2014;8(9):e3191. doi: 10.1371/journal.pntd.0003191. PubMed
700 PMID: 25254971; PubMed Central PMCID: PMCPMC4177881.
- 701 33. Shelite TR, Liang Y, Wang H, Mendell NL, Trent BJ, Sun J, et al. IL-33-Dependent
702 Endothelial Activation Contributes to Apoptosis and Renal Injury in *Orientia tsutsugamushi*-
703 Infected Mice. *PLoS Negl Trop Dis.* 2016;10(3):e0004467. doi: 10.1371/journal.pntd.0004467.
704 PubMed PMID: 26943125; PubMed Central PMCID: PMCPMC4778942.
- 705 34. Soong L, Shelite TR, Xing Y, Kodakandla H, Liang Y, Trent BJ, et al. Type 1-skewed
706 neuroinflammation and vascular damage associated with *Orientia tsutsugamushi* infection in
707 mice. *PLoS Negl Trop Dis.* 2017;11(7):e0005765. Epub 2017/07/24. doi:
708 10.1371/journal.pntd.0005765. PubMed PMID: 28742087; PubMed Central PMCID:
709 PMCPMC5542690.
- 710 35. Shelite TR, Saito TB, Mendell NL, Gong B, Xu G, Soong L, et al. Hematogenously
711 disseminated *Orientia tsutsugamushi*-infected murine model of scrub typhus [corrected]. *PLoS*
712 *Negl Trop Dis.* 2014;8(7):e2966. doi: 10.1371/journal.pntd.0002966. PubMed PMID: 25010338;
713 PubMed Central PMCID: PMCPMC4091938.
- 714 36. Gonzales JN, Lucas R, Verin AD. The Acute Respiratory Distress Syndrome:
715 Mechanisms and Perspective Therapeutic Approaches. *Austin J Vasc Med.* 2015;2(1). PubMed
716 PMID: 26973981; PubMed Central PMCID: PMCPMC4786180.

- 717 37. Heitrich M, García DM, Stoyanoff TR, Rodríguez JP, Todaro JS, Aguirre MV.
718 Erythropoietin attenuates renal and pulmonary injury in polymicrobial induced-sepsis through
719 EPO-R, VEGF and VEGF-R2 modulation. *Biomed Pharmacother.* 2016;82:606-13. Epub
720 2016/06/11. doi: 10.1016/j.biopha.2016.05.045. PubMed PMID: 27470403.
- 721 38. Ghosh CC, David S, Zhang R, Berghelli A, Milam K, Higgins SJ, et al. Gene control of
722 tyrosine kinase TIE2 and vascular manifestations of infections. *Proc Natl Acad Sci U S A.*
723 2016;113(9):2472-7. Epub 2016/02/16. doi: 10.1073/pnas.1519467113. PubMed PMID:
724 26884170; PubMed Central PMCID: PMC4780619.
- 725 39. Parikh SM. The Angiopoietin-Tie2 Signaling Axis in Systemic Inflammation. *J Am Soc*
726 *Nephrol.* 2017;28(7):1973-82. Epub 2017/05/02. doi: 10.1681/ASN.2017010069. PubMed
727 PMID: 28465380; PubMed Central PMCID: PMC4780619.
- 728 40. Xu G, Mendell NL, Liang Y, Shelite TR, Goetz-Rivillas Y, Soong L, et al. Correction:
729 CD8+ T cells provide immune protection against murine disseminated endotheliotropic *Orientia*
730 *tsutsugamushi* infection. *PLoS Negl Trop Dis.* 2017;11(12):e0006127. Epub 2017/12/06. doi:
731 10.1371/journal.pntd.0006127. PubMed PMID: 29211737; PubMed Central PMCID:
732 PMC4780619.
- 733 41. Hauptmann M, Kolbaum J, Lilla S, Wozniak D, Gharaibeh M, Fleischer B, et al.
734 Protective and Pathogenic Roles of CD8+ T Lymphocytes in Murine *Orientia tsutsugamushi*
735 Infection. *PLoS Negl Trop Dis.* 2016;10(9):e0004991. Epub 2016/09/08. doi:
736 10.1371/journal.pntd.0004991. PubMed PMID: 27606708; PubMed Central PMCID:
737 PMC4780619.
- 738 42. Tantibhedhyangkul W, Prachason T, Waywa D, El Filali A, Ghigo E, Thongnoppakhun
739 W, et al. *Orientia tsutsugamushi* stimulates an original gene expression program in monocytes:

740 relationship with gene expression in patients with scrub typhus. *PLoS Negl Trop Dis*.
741 2011;5(5):e1028. Epub 2011/05/17. doi: 10.1371/journal.pntd.0001028. PubMed PMID:
742 21610853; PubMed Central PMCID: PMC3096591.

743 43. Misharin AV, Morales-Nebreda L, Mutlu GM, Budinger GR, Perlman H. Flow
744 cytometric analysis of macrophages and dendritic cell subsets in the mouse lung. *Am J Respir*
745 *Cell Mol Biol*. 2013;49(4):503-10. doi: 10.1165/rcmb.2013-0086MA. PubMed PMID:
746 23672262; PubMed Central PMCID: PMC3824047.

747 44. Min CK, Kim HI, Ha NY, Kim Y, Kwon EK, Yen NTH, et al. A Type I Interferon and
748 IL-10 Induced by. *Front Immunol*. 2018;9:2022. Epub 2018/09/04. doi:
749 10.3389/fimmu.2018.02022. PubMed PMID: 30233599; PubMed Central PMCID:
750 PMC6131522.

751 45. Buchacher T, Ohradanova-Repic A, Stockinger H, Fischer MB, Weber V. M2
752 Polarization of Human Macrophages Favors Survival of the Intracellular Pathogen *Chlamydia*
753 *pneumoniae*. *PLoS One*. 2015;10(11):e0143593. Epub 2015/11/25. doi:
754 10.1371/journal.pone.0143593. PubMed PMID: 26606059; PubMed Central PMCID:
755 PMC4659546.

756 46. Ying W, Cheruku PS, Bazer FW, Safe SH, Zhou B. Investigation of macrophage
757 polarization using bone marrow derived macrophages. *J Vis Exp*. 2013;(76). Epub 2013/06/23.
758 doi: 10.3791/50323. PubMed PMID: 23851980; PubMed Central PMCID: PMC3728835.

759 47. Rothlein R, Dustin ML, Marlin SD, Springer TA. A human intercellular adhesion
760 molecule (ICAM-1) distinct from LFA-1. *J Immunol*. 1986;137(4):1270-4. PubMed PMID:
761 3525675.

- 762 48. Paris DH, Jenjaroen K, Blacksell SD, Phetsouvanh R, Wuthiekanun V, Newton PN, et al.
763 Differential patterns of endothelial and leucocyte activation in 'typhus-like' illnesses in Laos and
764 Thailand. *Clin Exp Immunol.* 2008;153(1):63-7. Epub 2008/05/23. doi: 10.1111/j.1365-
765 2249.2008.03673.x. PubMed PMID: 18505434; PubMed Central PMCID: PMCPMC2432098.
- 766 49. Dejana E, Orsenigo F, Lampugnani MG. The role of adherens junctions and VE-cadherin
767 in the control of vascular permeability. *J Cell Sci.* 2008;121(Pt 13):2115-22. doi:
768 10.1242/jcs.017897. PubMed PMID: 18565824.
- 769 50. Coon BG, Baeyens N, Han J, Budatha M, Ross TD, Fang JS, et al. Intramembrane
770 binding of VE-cadherin to VEGFR2 and VEGFR3 assembles the endothelial mechanosensory
771 complex. *J Cell Biol.* 2015;208(7):975-86. Epub 2015/03/23. doi: 10.1083/jcb.201408103.
772 PubMed PMID: 25800053; PubMed Central PMCID: PMCPMC4384728.
- 773 51. Dumont DJ, Gradwohl G, Fong GH, Puri MC, Gertsenstein M, Auerbach A, et al.
774 Dominant-negative and targeted null mutations in the endothelial receptor tyrosine kinase, tek,
775 reveal a critical role in vasculogenesis of the embryo. *Genes Dev.* 1994;8(16):1897-909. doi:
776 10.1101/gad.8.16.1897. PubMed PMID: 7958865.
- 777 52. Jeansson M, Gawlik A, Anderson G, Li C, Kerjaschki D, Henkelman M, et al.
778 Angiopoietin-1 is essential in mouse vasculature during development and in response to injury. *J*
779 *Clin Invest.* 2011;121(6):2278-89. doi: 10.1172/JCI46322. PubMed PMID: 21606590; PubMed
780 Central PMCID: PMCPMC3104773.
- 781 53. David S, Park JK, Meurs M, Zijlstra JG, Koenecke C, Schimpf C, et al. Acute
782 administration of recombinant Angiopoietin-1 ameliorates multiple-organ dysfunction syndrome
783 and improves survival in murine sepsis. *Cytokine.* 2011;55(2):251-9. Epub 2011/04/30. doi:
784 10.1016/j.cyto.2011.04.005. PubMed PMID: 21531574.

- 785 54. Stiehl T, Thamm K, Kaufmann J, Schaeper U, Kirsch T, Haller H, et al. Lung-targeted
786 RNA interference against angiotensin-2 ameliorates multiple organ dysfunction and death in
787 sepsis. *Crit Care Med.* 2014;42(10):e654-62. doi: 10.1097/CCM.0000000000000524. PubMed
788 PMID: 25083983.
- 789 55. Phanthanawiboon S, Limkittikul K, Sakai Y, Takakura N, Saijo M, Kurosu T. Acute
790 Systemic Infection with Dengue Virus Leads to Vascular Leakage and Death through Tumor
791 Necrosis Factor- α and Tie2/Angiotensin Signaling in Mice Lacking Type I and II Interferon
792 Receptors. *PLoS One.* 2016;11(2):e0148564. Epub 2016/02/04. doi:
793 10.1371/journal.pone.0148564. PubMed PMID: 26844767; PubMed Central PMCID:
794 PMCPMC4742241.
- 795 56. Higgins SJ, Purcell LA, Silver KL, Tran V, Crowley V, Hawkes M, et al. Dysregulation
796 of angiotensin-1 plays a mechanistic role in the pathogenesis of cerebral malaria. *Sci Transl*
797 *Med.* 2016;8(358):358ra128. doi: 10.1126/scitranslmed.aaf6812. PubMed PMID: 27683553.
- 798 57. Curto P, Simões I, Riley SP, Martinez JJ. Differences in Intracellular Fate of Two
799 Spotted Fever Group Rickettsia in Macrophage-Like Cells. *Front Cell Infect Microbiol.*
800 2016;6:80. Epub 2016/07/29. doi: 10.3389/fcimb.2016.00080. PubMed PMID: 27525249;
801 PubMed Central PMCID: PMCPMC4965480.
- 802 58. Aggarwal NR, King LS, D'Alessio FR. Diverse macrophage populations mediate acute
803 lung inflammation and resolution. *Am J Physiol Lung Cell Mol Physiol.* 2014;306(8):L709-25.
804 Epub 2014/02/07. doi: 10.1152/ajplung.00341.2013. PubMed PMID: 24508730; PubMed
805 Central PMCID: PMCPMC3989724.
- 806 59. Garcia S, Krausz S, Ambarus CA, Fernandez BM, Hartkamp LM, van Es IE, et al. Tie2
807 signaling cooperates with TNF to promote the pro-inflammatory activation of human

- 808 macrophages independently of macrophage functional phenotype. PLoS One. 2014;9(1):e82088.
809 doi: 10.1371/journal.pone.0082088. PubMed PMID: 24404127; PubMed Central PMCID:
810 PMCPMC3880273.
- 811 60. Díaz FE, Abarca K, Kalergis AM. An Update on Host-Pathogen Interplay and
812 Modulation of Immune Responses during *Orientia tsutsugamushi* Infection. Clin Microbiol Rev.
813 2018;31(2). Epub 2018/01/31. doi: 10.1128/CMR.00076-17. PubMed PMID: 29386235;
814 PubMed Central PMCID: PMCPMC5967693.
- 815 61. Tsai MH, Chang CH, Tsai RK, Hong YR, Chuang TH, Fan KT, et al. Cross-Regulation
816 of Proinflammatory Cytokines by Interleukin-10 and miR-155 in *Orientia tsutsugamushi*-
817 Infected Human Macrophages Prevents Cytokine Storm. J Invest Dermatol. 2016;136(7):1398-
818 407. Epub 2016/02/24. doi: 10.1016/j.jid.2015.11.034. PubMed PMID: 26921773.
- 819 62. Soong L, Mendell NL, Olano JP, Rockx-Brouwer D, Xu G, Goetz-Rivillas Y, et al. An
820 Intradermal Inoculation Mouse Model for Immunological Investigations of Acute Scrub Typhus
821 and Persistent Infection. PLoS Negl Trop Dis. 2016;10(8):e0004884. Epub 2016/08/01. doi:
822 10.1371/journal.pntd.0004884. PubMed PMID: 27479584; PubMed Central PMCID:
823 PMCPMC4968841.
- 824 63. Lurchachaiwong W, Monkanna T, Leepitakrat S, Ponlawat A, Sattabongkot J, Schuster
825 AL, et al. Variable clinical responses of a scrub typhus outbred mouse model to feeding by
826 *Orientia tsutsugamushi* infected mites. Exp Appl Acarol. 2012;58(1):23-34. Epub 2012/04/24.
827 doi: 10.1007/s10493-012-9563-8. PubMed PMID: 22527840.
- 828 64. Mendell NL, Bouyer DH, Walker DH. Murine models of scrub typhus associated with
829 host control of *Orientia tsutsugamushi* infection. PLoS Negl Trop Dis. 2017;11(3):e0005453.

830 Epub 2017/03/10. doi: 10.1371/journal.pntd.0005453. PubMed PMID: 28282373; PubMed
831 Central PMCID: PMCPMC5362142.

832 65. Singer BD, Mock JR, D'Alessio FR, Aggarwal NR, Mandke P, Johnston L, et al. Flow-
833 cytometric method for simultaneous analysis of mouse lung epithelial, endothelial, and
834 hematopoietic lineage cells. *Am J Physiol Lung Cell Mol Physiol*. 2016;310(9):L796-801. Epub
835 2016/03/04. doi: 10.1152/ajplung.00334.2015. PubMed PMID: 26944088; PubMed Central
836 PMCID: PMCPMC4867353.

837 66. Gong B, Shelite T, Mei FC, Ha T, Hu Y, Xu G, et al. Exchange protein directly activated
838 by cAMP plays a critical role in bacterial invasion during fatal rickettsioses. *Proc Natl Acad Sci*
839 *U S A*. 2013;110(48):19615-20. Epub 2013/11/11. doi: 10.1073/pnas.1314400110. PubMed
840 PMID: 24218580; PubMed Central PMCID: PMCPMC3845138.

841

842

843

844

845

846

847

848

849

850

851

852

853 **Figure Legends**

854

855 **Fig 1. Endothelial cell (EC) activation and vascular damage in the lungs of *O.***

856 ***tsutsugamushi*-infected mice and in infected HUVECs *in vitro*.** Female C57BL/6J mice were

857 inoculated with 1.325×10^6 of *O. tsutsugamushi* Karp strain (4-5 mice/group) or PBS (3-4

858 mice/group). At days 2, 6, or 9 post-infection, equivalent lung portions were collected for

859 analyses. (A) Frozen lung sections were co-stained for *Orientia* bacteria (red), ICAM-1 (green),

860 and DAPI (blue, top row, scale bar = 50 μ m) with close-up views of the boxed areas in the

861 bottom row (bar = 20 μ m). (B) Lung sections were co-stained for VE-cadherin (adherens

862 junctions, red), FITC-labeled I-B₄ lectins (green), and DAPI (blue, top row, bars = 50 μ m).

863 Close-up views of the boxed areas located the bottom row (bar = 20 μ m). (C) Quantification of

864 fluorescent ICAM-1 and VE-Cadherin staining (four images per time point). (D) Lung-derived

865 cells were analyzed via flow cytometry for the percentage of ICAM-1⁺ and VEGFR2⁺ cells

866 among gated CD31⁺CD45⁻ ECs (4-5 mice/group in infected groups; 3 mice/group in PBS

867 groups). *, $p < 0.05$; **, $p < 0.01$; and ***, $p < 0.001$; ****, $p < 0.0001$ compared to PBS controls.

868 Graphs are shown as mean +/- SEM. Flow cytometric and qRT-PCR data were analyzed by

869 using one-way ANOVA with Tukey's Post Hoc. At least 4 independent mouse infection

870 experiments and 2 independent *in vitro* experiments were performed with similar trends, and

871 shown are representative data.

872

873 **Fig 2. Elevated Ang2 expression and decreased Ang1 expression during *O. tsutsugamushi***

874 **infection.** Mice were infected as in *Fig. 1*. (A) Frozen lung sections were co-stained for Ang1 (a

875 marker for endothelial quiescence, green), Ang2 (an endothelial stress marker, red), and DAPI

876 (blue) showing images at a low magnification (top row, scale bar = 50 μm) and close-up views
877 of the boxed areas (bottom row, bar = 20 μm). (B) Quantification of fluorescent Ang1 and Ang2
878 staining (four images per time point). (C) Human serum Ang2 proteins in the control subjects
879 (CNT) or scrub typhus patients (8/group) with different anti-*Orientia* IFA antibody titers were
880 measured by ELISA. Shown are data from two independent experiments. *, $p < 0.05$; **, $p <$
881 0.01 and ***, $p < 0.001$; ****, $p < 0.0001$ compared to the controls. Graphs are shown as mean +/-
882 SEM. Serum ELISA and qRT-PCR groups were analyzed via one-way ANOVA with Tukey's
883 Post Hoc. At least 3 independent mouse infection experiments were performed with similar
884 trends, and shown are representative data.

885 **Fig 3. Reduced Tie2 expression and activation in the lungs of *O. tsutsugamushi* infected**
886 **mice.** Frozen lung tissue sections were stained for the Tie2 receptor (red) and DAPI (blue, bar =
887 50 μm). (B) Lung tissue homogenates (40 $\mu\text{g}/\text{lane}$) were measured by Western blots for the
888 levels of phospho-Tie2 (pTie2) and total Tie2 proteins and compared with the GAPDH controls.
889 (C) *TIE2* mRNA levels in mouse lungs were measured via qRT-PCR; data are presented as
890 relative mRNA values normalized to GAPDH. **, $p < 0.01$ compared to the controls. Graph
891 shown as mean +/- SEM. Serum ELISA and qRT-PCR groups were analyzed via one-way
892 ANOVA with Tukey's Post Hoc.

893 **Fig 4. Polarized M Φ activation in infected mouse lungs.** Mice were infected with *O.*
894 *tsutsugamushi* (4-5 mice/group) or PBS (3-4 mice/group) for lung tissues collection at indicated
895 days of infection, as in *Fig. 1*. (A) Flow cytometric analyses of lung-derived cells, gated on
896 CD11b⁺Ly6G⁻ M Φ s and M Φ subsets, are shown for the D9 samples. The percentages and total
897 numbers of (B) activated M Φ s (CD64⁺CD11b⁺Ly6G⁻), (C) M1-type M Φ s

898 (CD80⁺CD64⁺CD11b⁺Ly6G⁻), as well as (D) M2-type MΦs (CD206⁺CD64⁺CD11b⁺Ly6G⁻) are
899 shown, respectively.

900 **Fig 5. Transcription of M1 and M2 associated genes in the lung of infected mice.** Lung
901 tissues were measured for the expression of M1-related genes (A) and M2-related genes (B),
902 respectively. Data are presented as relative to β-actin values. *, $p < 0.05$; **, $p < 0.01$; ***, $p <$
903 0.001 compared to the PBS controls. Graphs are shown as mean +/- SEM. One-way ANOVA
904 with Tukey's Post Hoc was used for statistical analysis. Two independent mouse infection
905 experiments were performed with similar trends, and shown are representative data.

906

907 **Fig 6. Enhanced bacterial growth in M2-polarized MΦs.** Bone marrow-derived MΦs were
908 generated from C57BL/6J mice, polarized into M1 or M2 types by pre-treatment of cells with
909 LPS (100 ng/ml) or rIL-4 (10 ng/ml), and infected with bacteria (5 MOI). (A) Bacterial loads at
910 3, 48, and 72 hpi (n = 5) were determined by qPCR. Data are presented as the *Orientia* 47-kDa
911 gene copy per pg of DNA. (B) Cells were co-stained for *Orientia* (green), IBA-1 (a MΦ marker,
912 red), and DAPI (blue) at 3 and 72 hpi. *, $p < 0.05$. Data for qPCR were analyzed via a Mann-
913 Whitney t test. Three independent experiments were performed with similar trends, and shown
914 are representative data.

915

916 **Supporting information**

917 **S1 Fig. Pulmonary pathology progression and reduced expression of occludin tight**
918 **junction proteins in infected lung tissues.** Female C57BL/6J mice (4-6 mice/group) were

919 inoculated with 1.325×10^6 of *O. tsutsugamushi* Karp strain. At indicated days of infection,
920 equivalent lung portions were collected. (A) Hematoxylin and eosin staining of lung tissues
921 during lethal challenge demonstrating increased cellular infiltration and alveolar thickening as
922 the infection progresses (scale bars = 50 μm). (B) Frozen sections were processed for
923 immunofluorescent staining and co-stained for occludin (cell-cell tight junctions, red), FITC-
924 labeled GSL I-B₄ lectins (green, top rows, scale bars = 50 μm), and DAPI (blue). The close-up
925 views of the boxed areas are shown in the lower row (bar = 20 μm). (C) Flow cytometry analysis
926 of viable pulmonary ECs (CD31⁺CD45⁻) collected at early (D0) and late (D9) infection. (D)
927 Cultured HUVECs were infected with bacteria at 3 or 10 multiplicity of infection (MOI, 4
928 samples/group) and analyzed via qRT-PCR for gene expression at 24 h post-infection. Data are
929 presented as relative to GAPDH values. *, $p < 0.05$; **, $p < 0.01$; and ***, $p < 0.001$ compared
930 to PBS controls. Graphs are shown as mean \pm SEM. Flow cytometric and qRT-PCR data were
931 analyzed by using one-way ANOVA with Tukey's Post Hoc. At least 3 independent mouse
932 infection experiments and 2 independent *in vitro* experiments were performed with similar
933 trends, and shown are representative data.

934

935 **S2 Fig. Leukocyte and T cell recruitment in the lungs of lethally challenged mice.** Female
936 C57BL/6J mice (3-5 mice per group) were inoculated with 1.325×10^6 of *O. tsutsugamushi* Karp
937 strain. At indicated days of infection, equivalent lung portions were collected and processed for
938 immunofluorescent staining or flow cytometric analysis. (A) Frozen sections were either co-
939 stained for Ang2 (red) and CD45 (a leukocyte marker, green), or Ang2 (green) and CD3 (a T cell
940 marker, red, bars = 50 μm). The percentage and absolute number of CD3⁺CD4⁺ T cells (B), as
941 well as CD3⁺CD8⁺ T cells (C), were quantified and compared to non-infected controls

942 (*, $p < 0.05$; **, $p < 0.01$; ****, $p < 0.0001$). Graphs are shown as +/- SEM. Flow cytometry groups
943 were analyzed using one-way ANOVA with Tukey's Post Hoc.

944

945 **S3 Fig. MΦ infection in mouse lungs and differentiation *in vitro*.** (A) Female C57BL/6J mice
946 (4-6 mice per group) were inoculated with 1.325×10^6 of *O. tsutsugamushi* Karp strain. At days
947 2 and 10, equivalent lung portions were processed; frozen sections were co-stained for *Orientia*
948 (red), IBA-1 (green, a macrophage marker), and DAPI (blue), showing images in a low-
949 magnification (top rows, scale bar = 50 μm) and close-up views of the boxed areas (bottom rows,
950 bar = 20 μm). (B) Bone marrow-derived MΦs were treated with LPS (100 ng/ml) or rIL-4 (10
951 ng/ml) for 24 h and analyzed for the expression of indicated markers via flow cytometry. The
952 numbers represent the percentages (%) of gated cells. (C) LPS- and IL-4-primed cells were
953 analyzed by qRT-PCR for the expression of the indicated markers, showing the polarization of
954 MΦ subsets compared with control cells (*, $p < 0.05$; **, $p < 0.01$; and ****, $p < 0.0001$). Data
955 are shown as +/- SEM and were analyzed using one-way ANOVA with Tukey's Post Hoc.

956 **S1 Table. Real-time PCR primers of human, murine, and bacterial genes.** The primer
957 sequences used in this study (listed in the 5' to 3' direction).

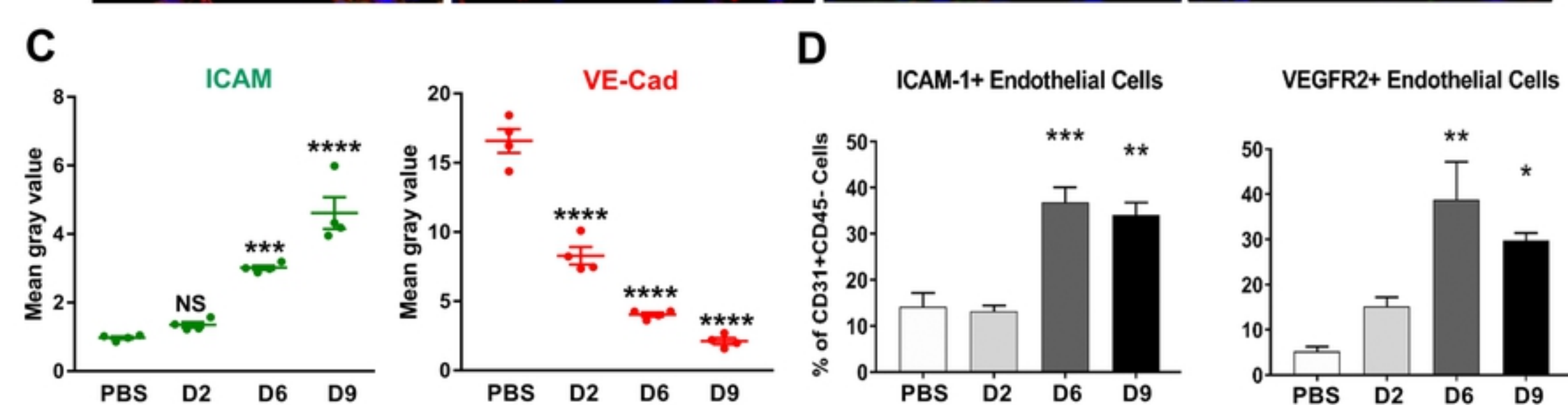
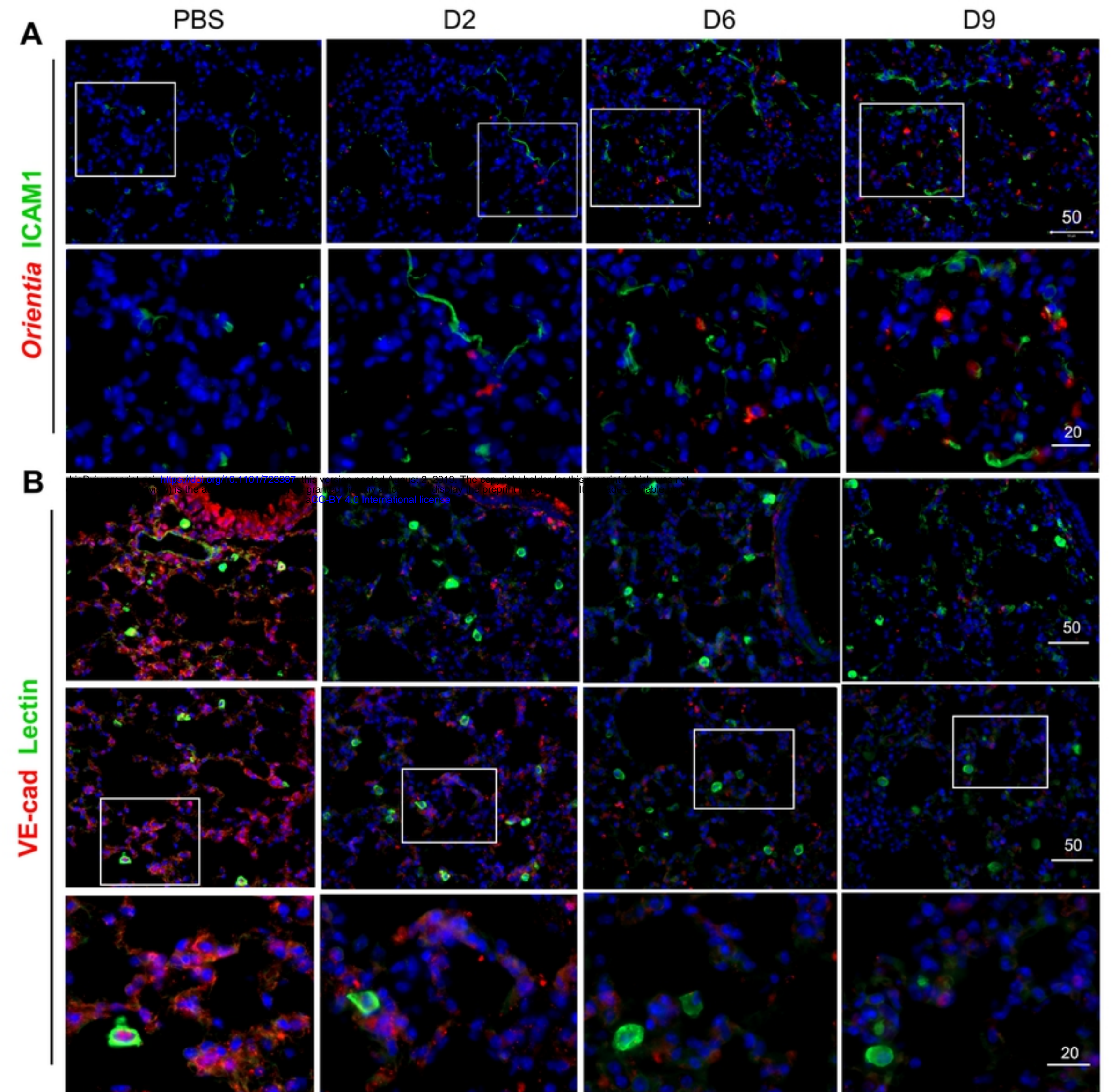


Figure 1

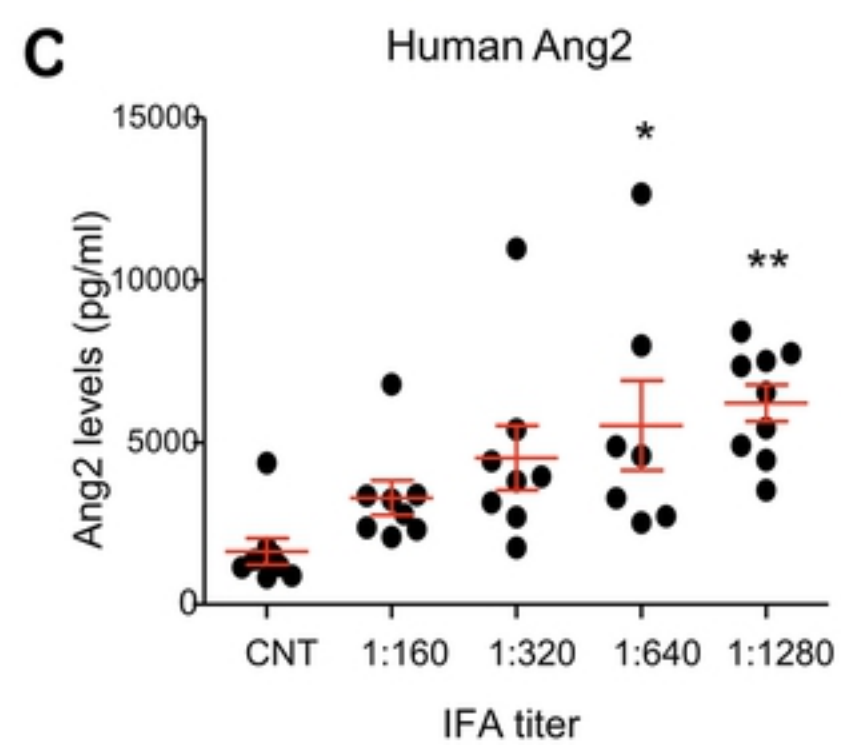
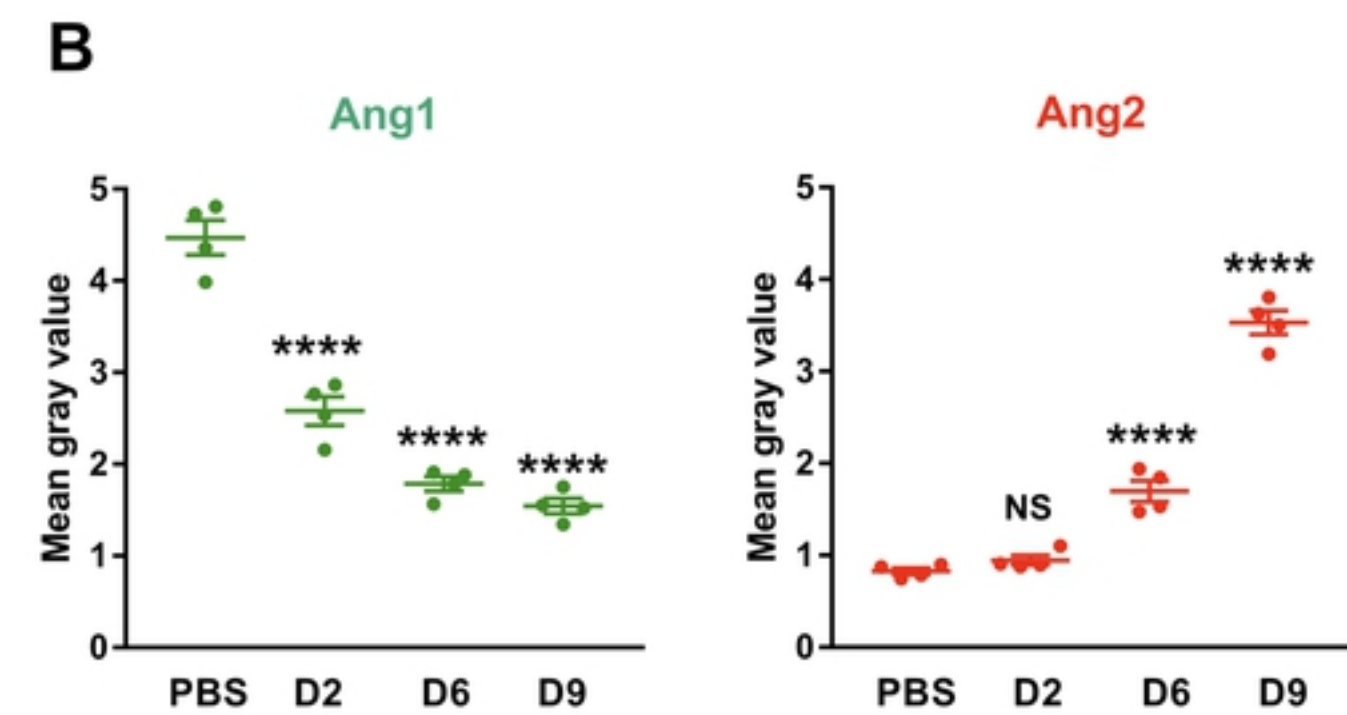
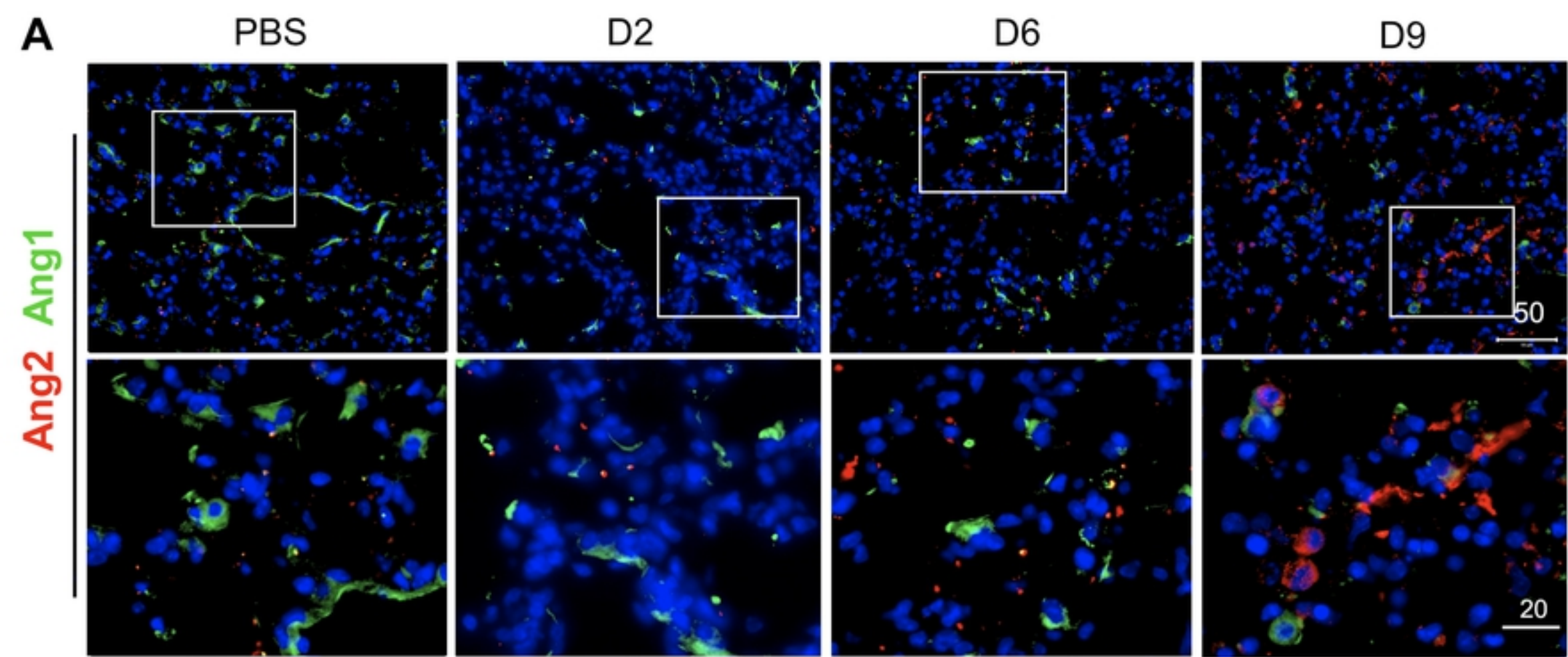


Figure 2

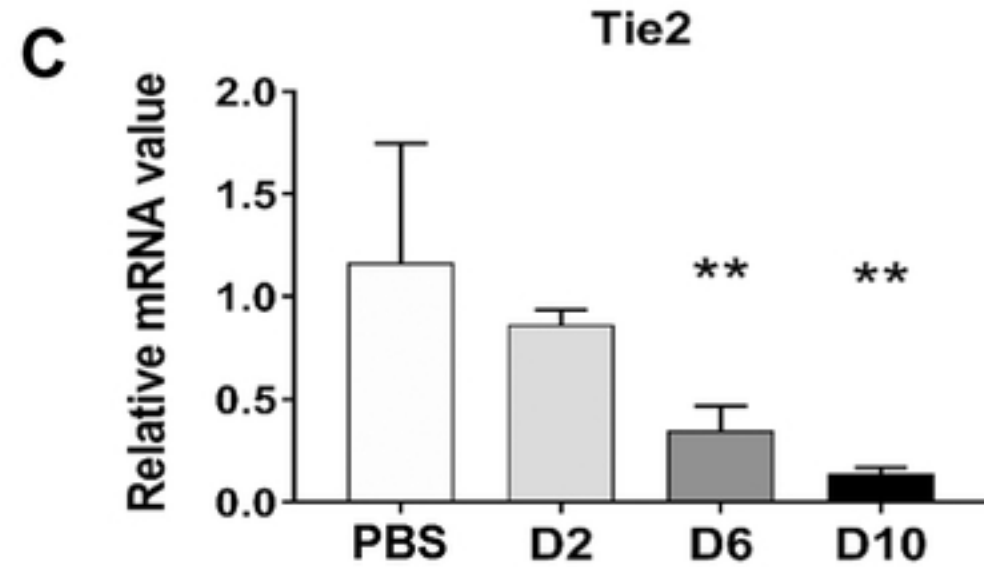
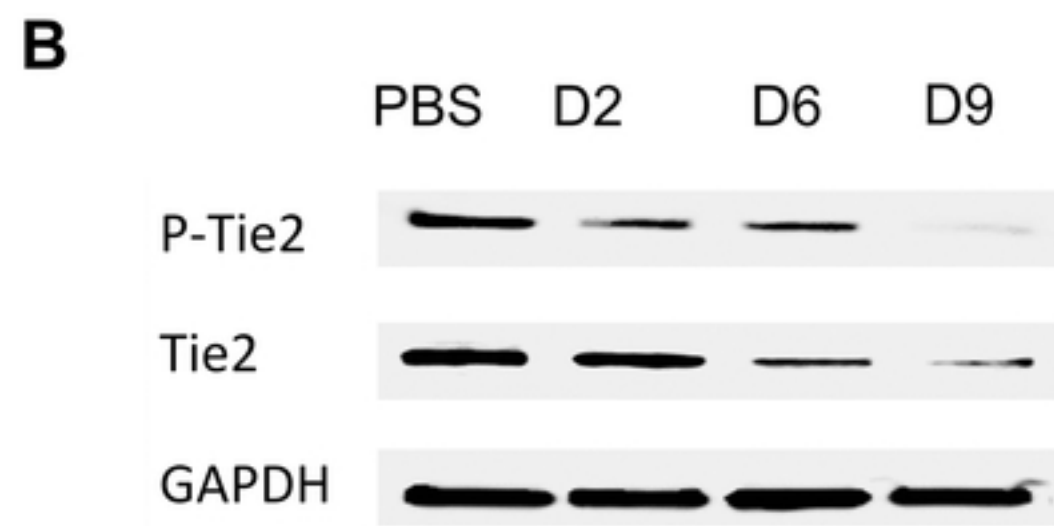
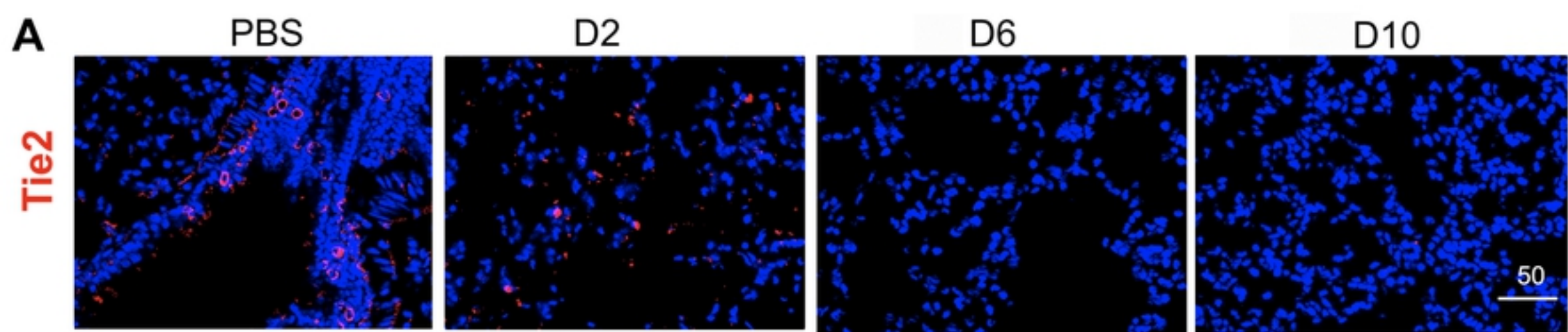


Figure 3

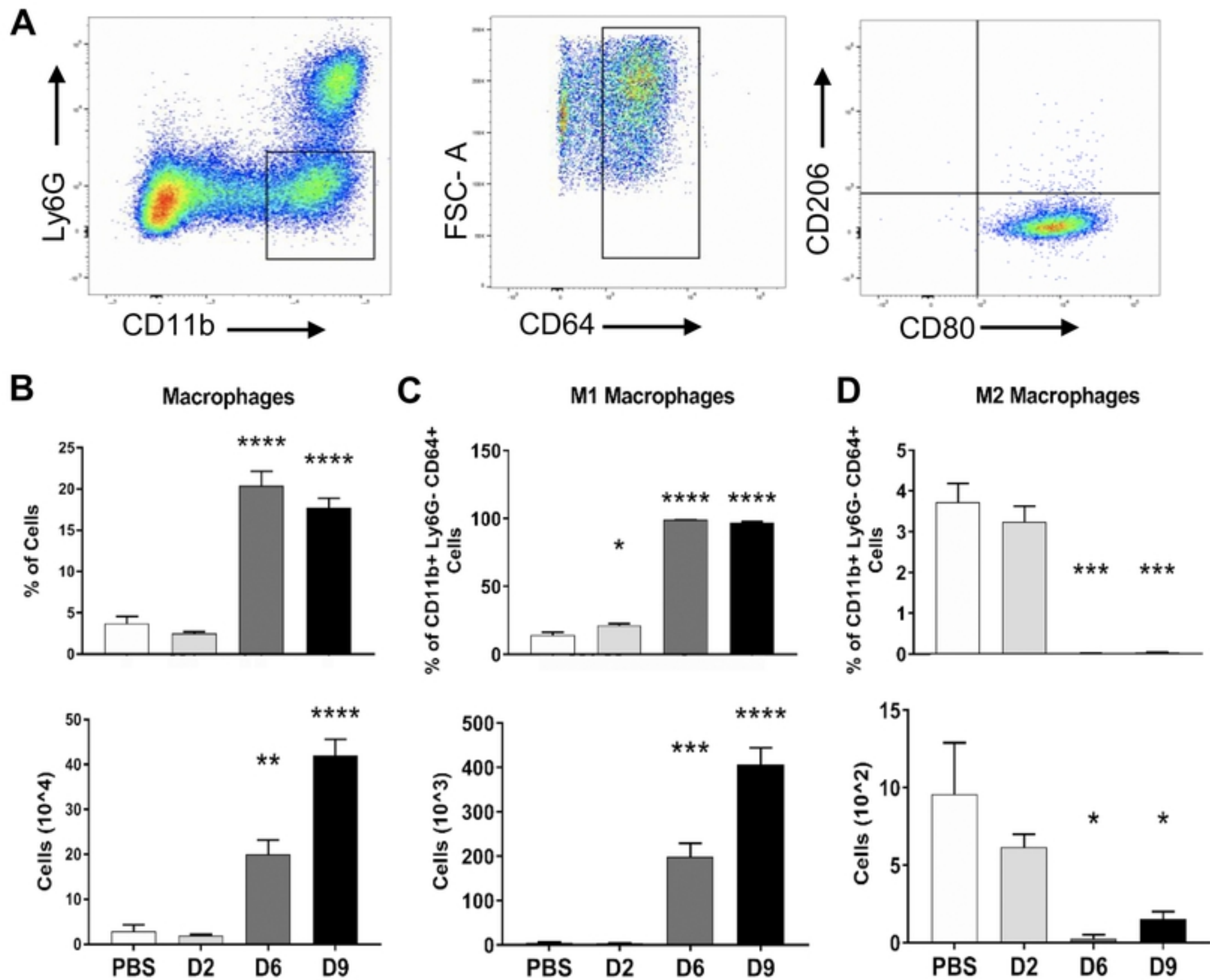


Figure 4

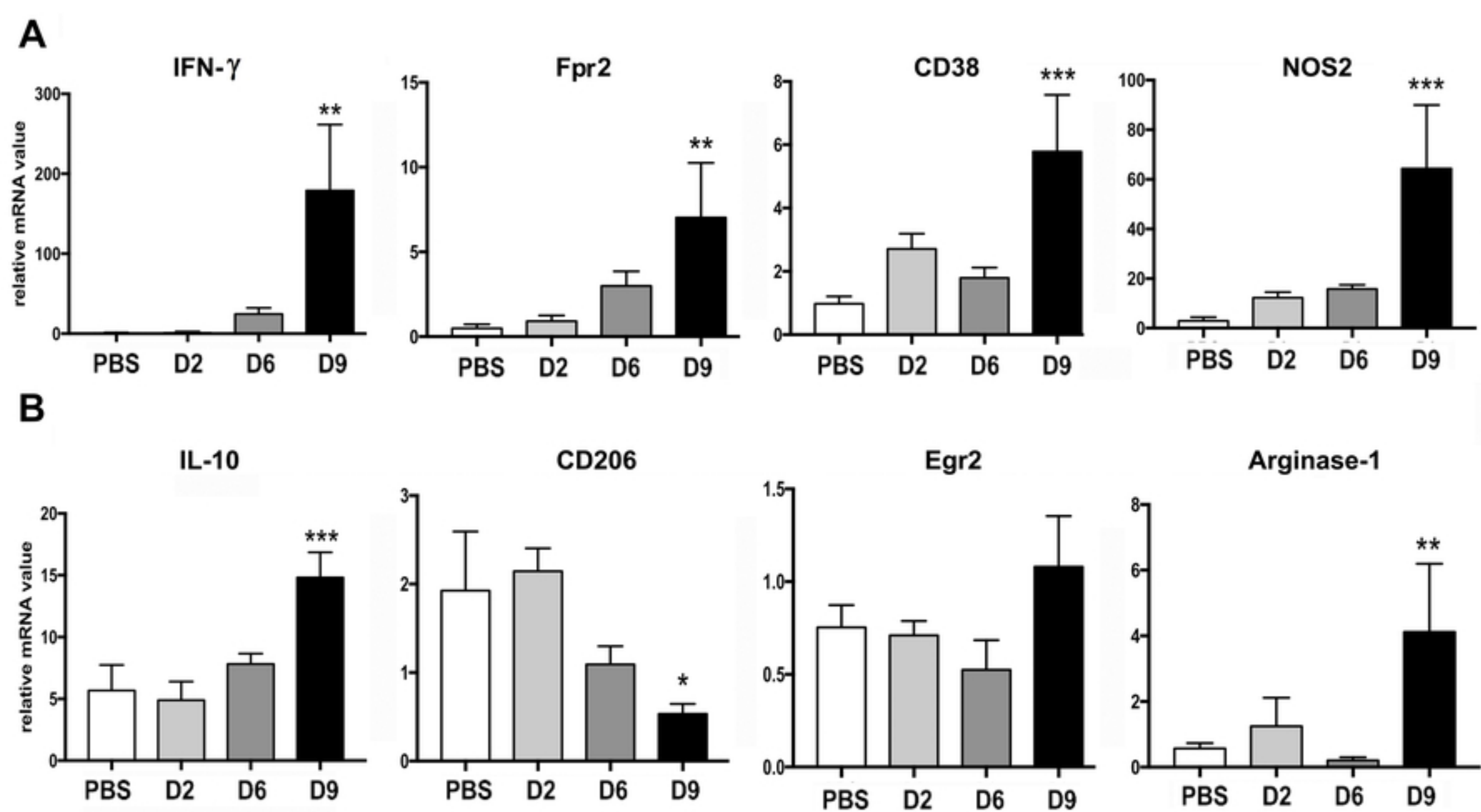


Figure 5

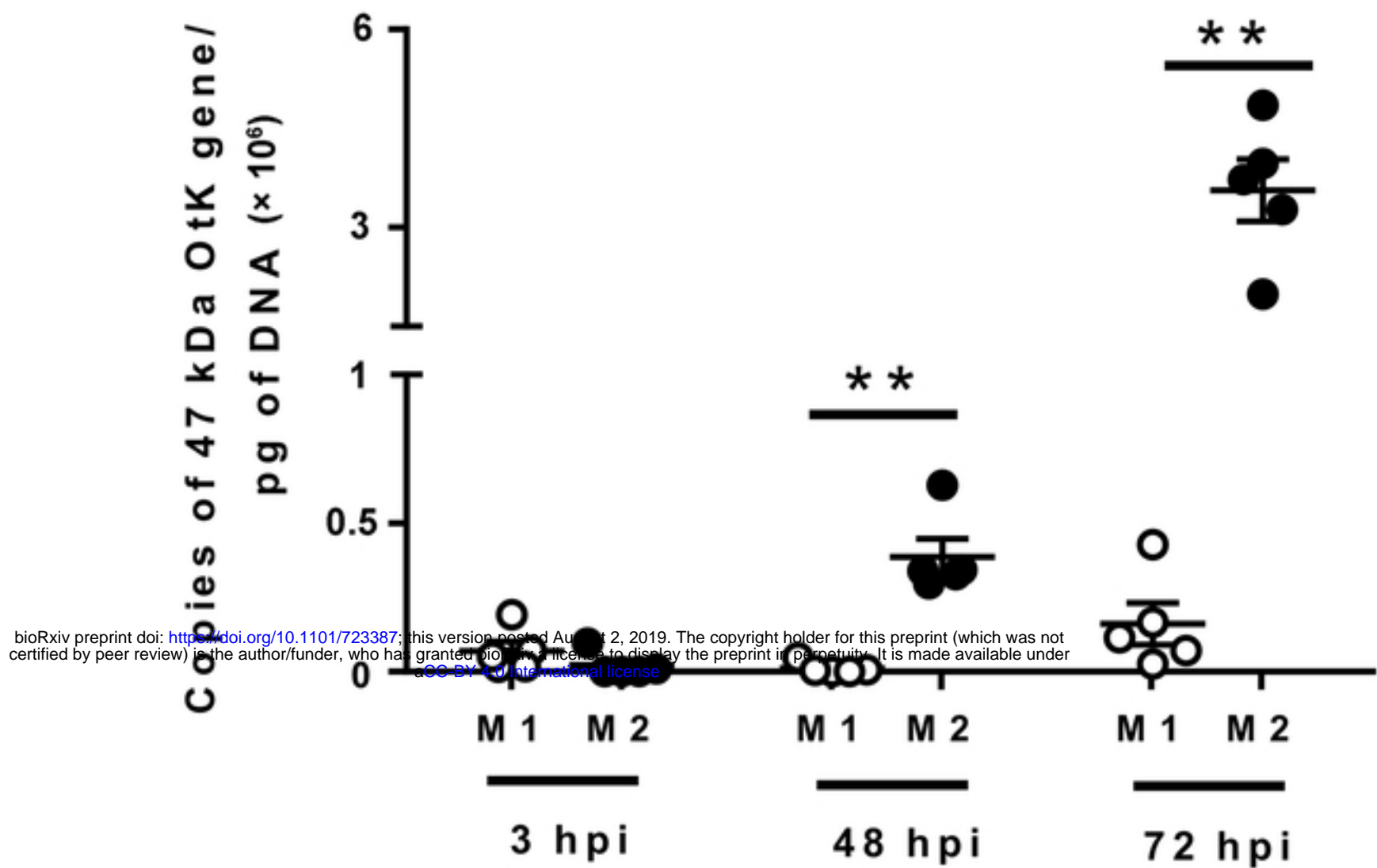
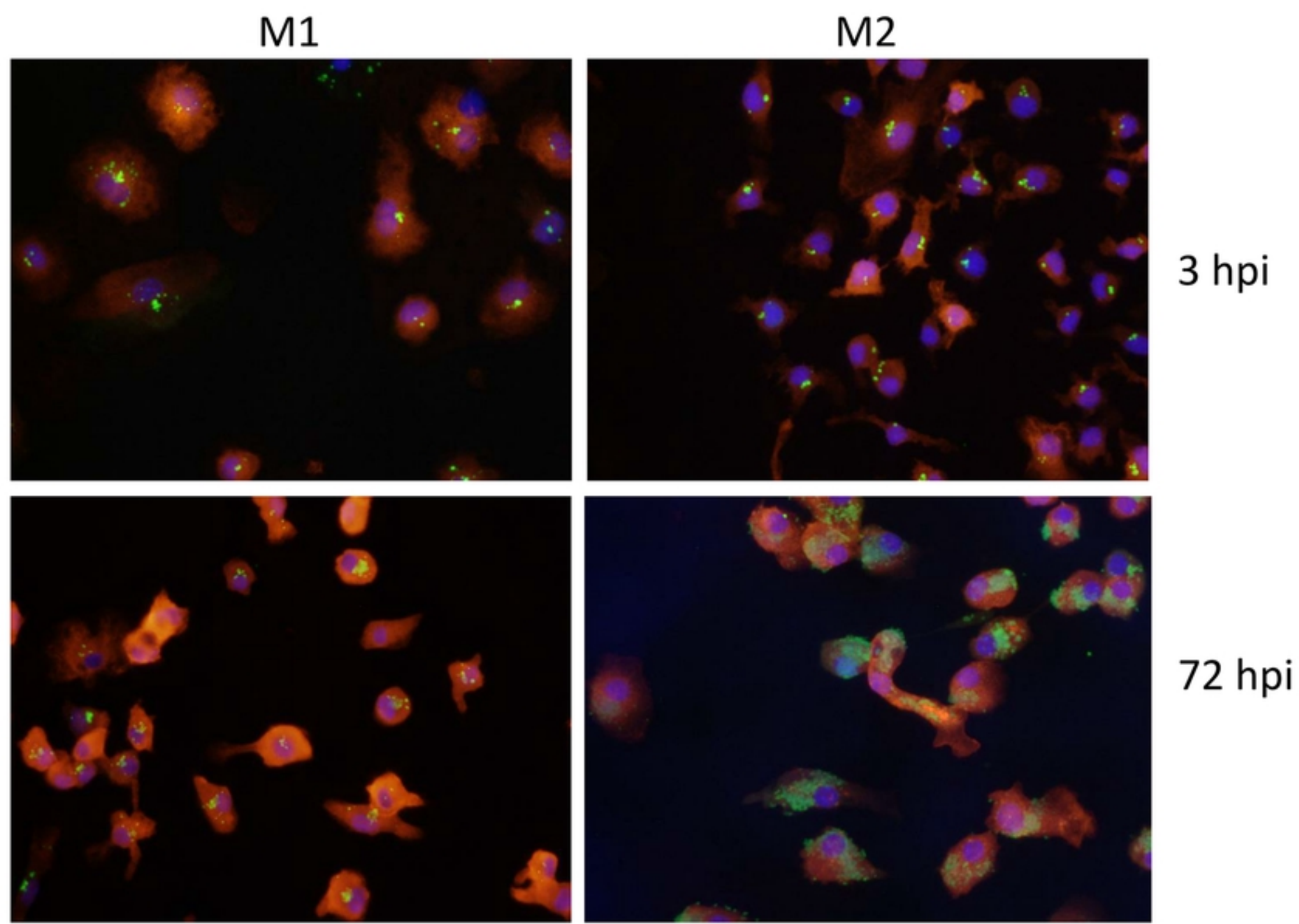
A**B**

Figure 6

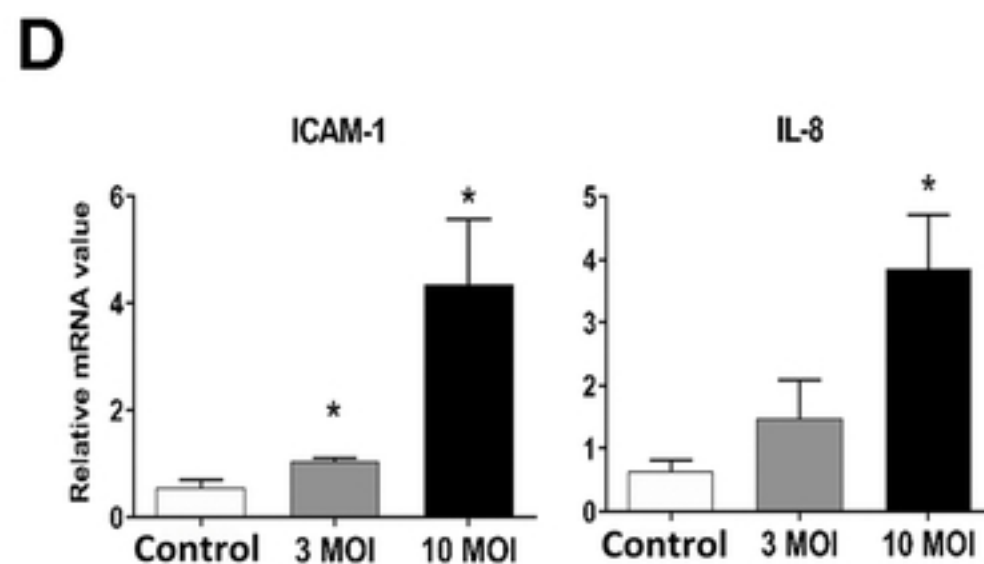
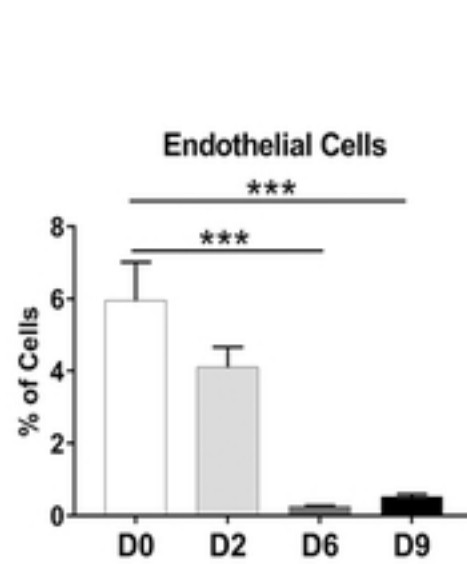
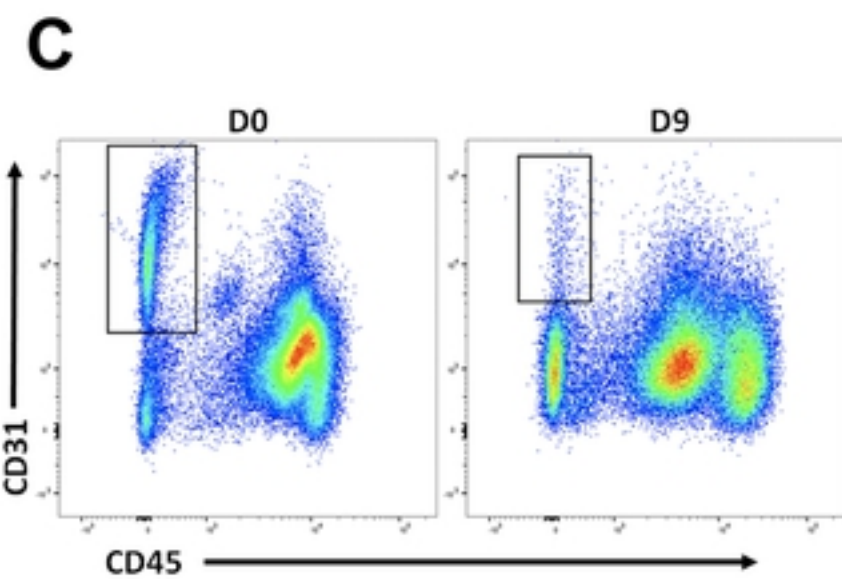
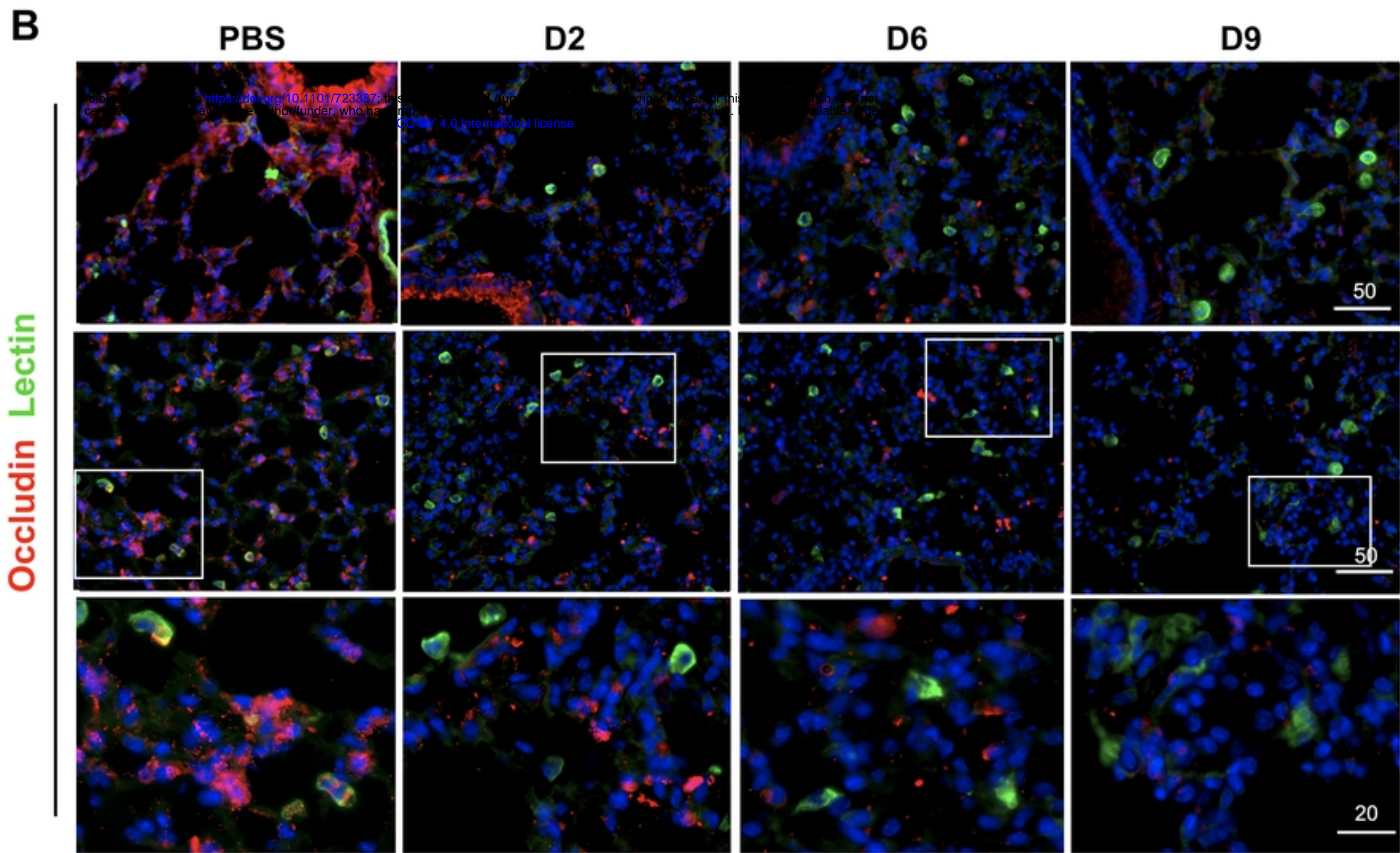
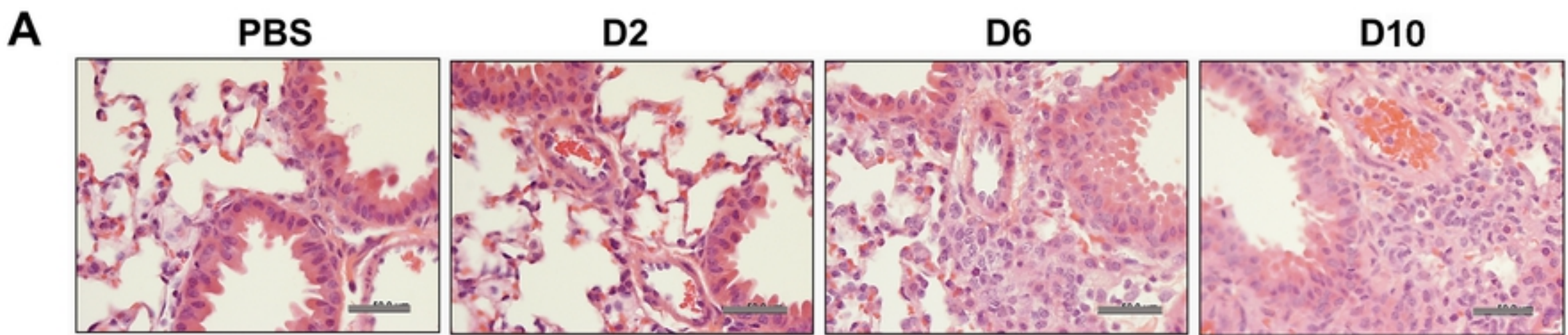


Figure S1

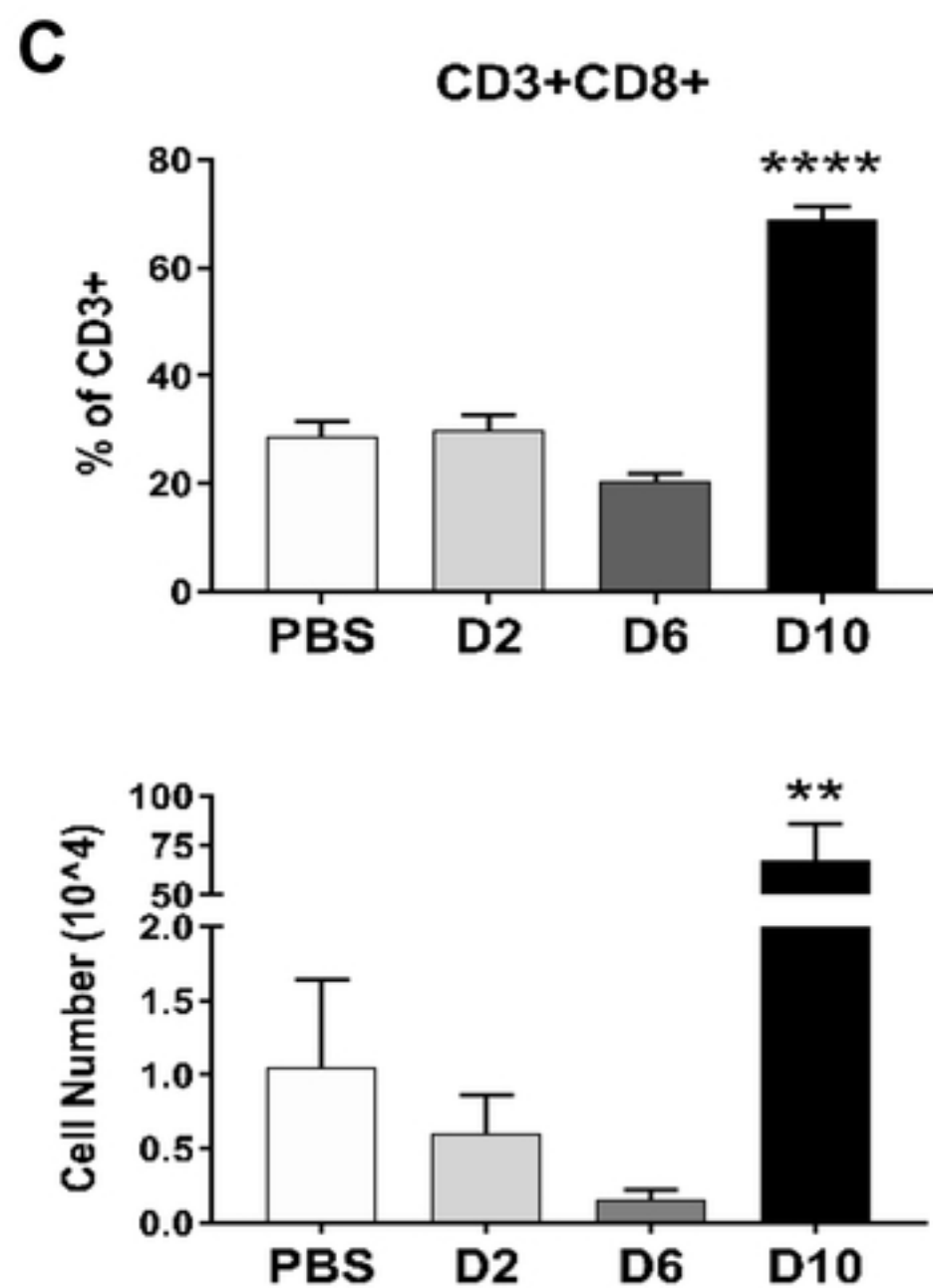
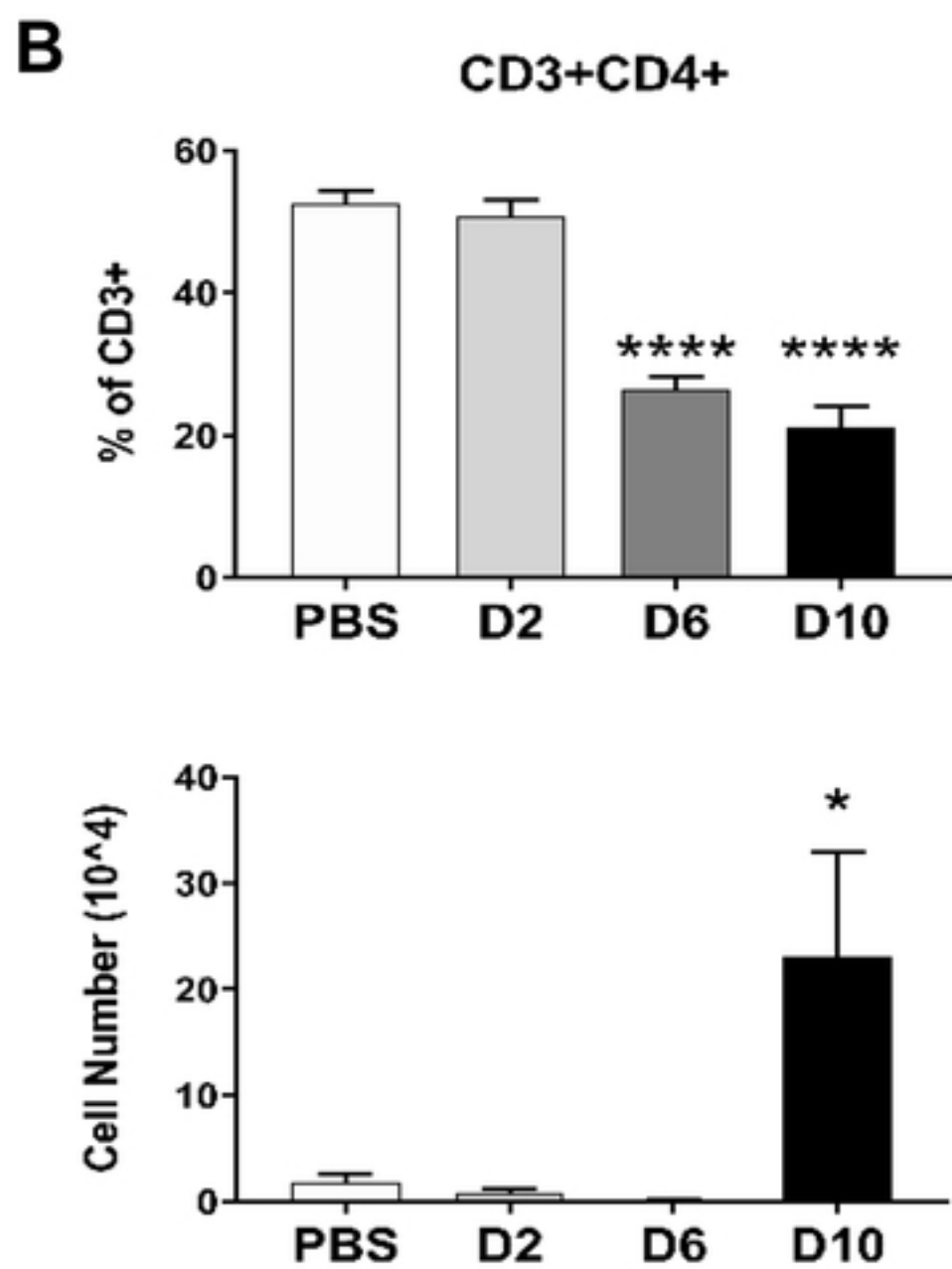
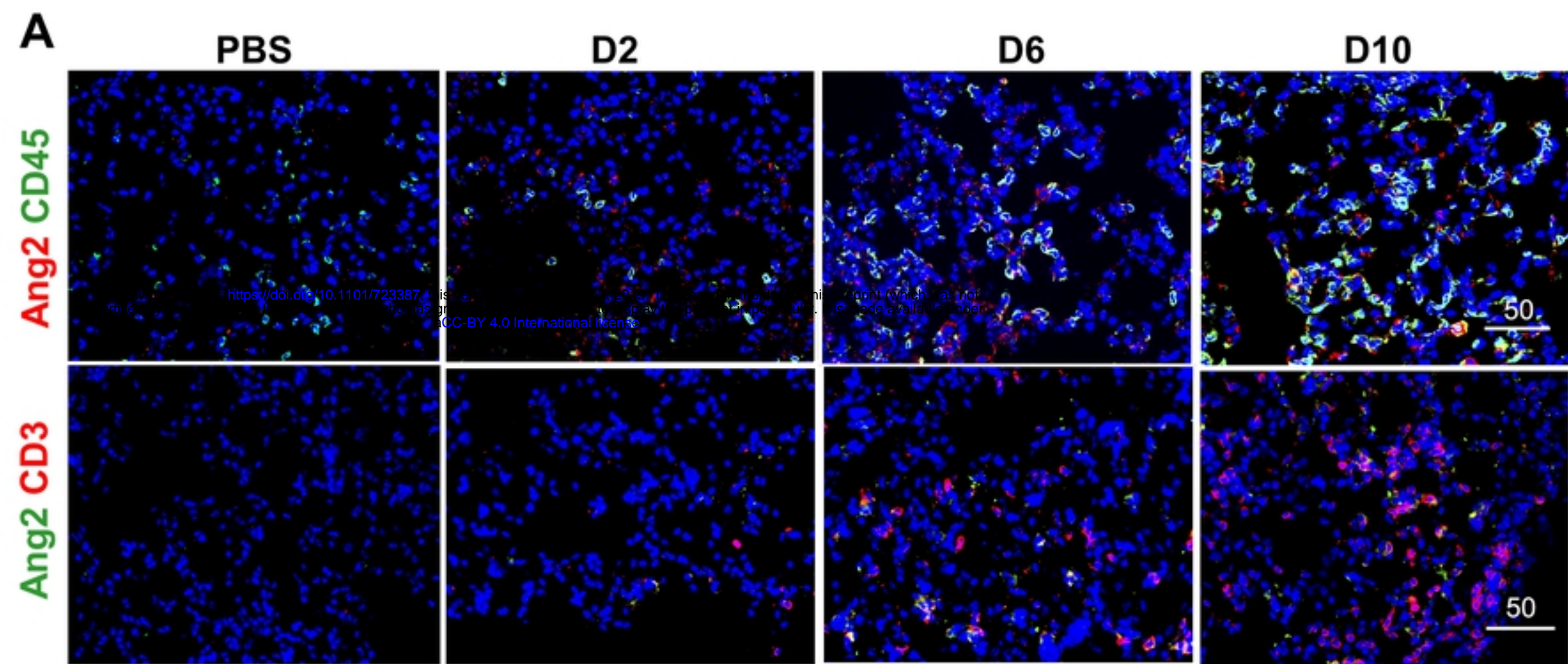
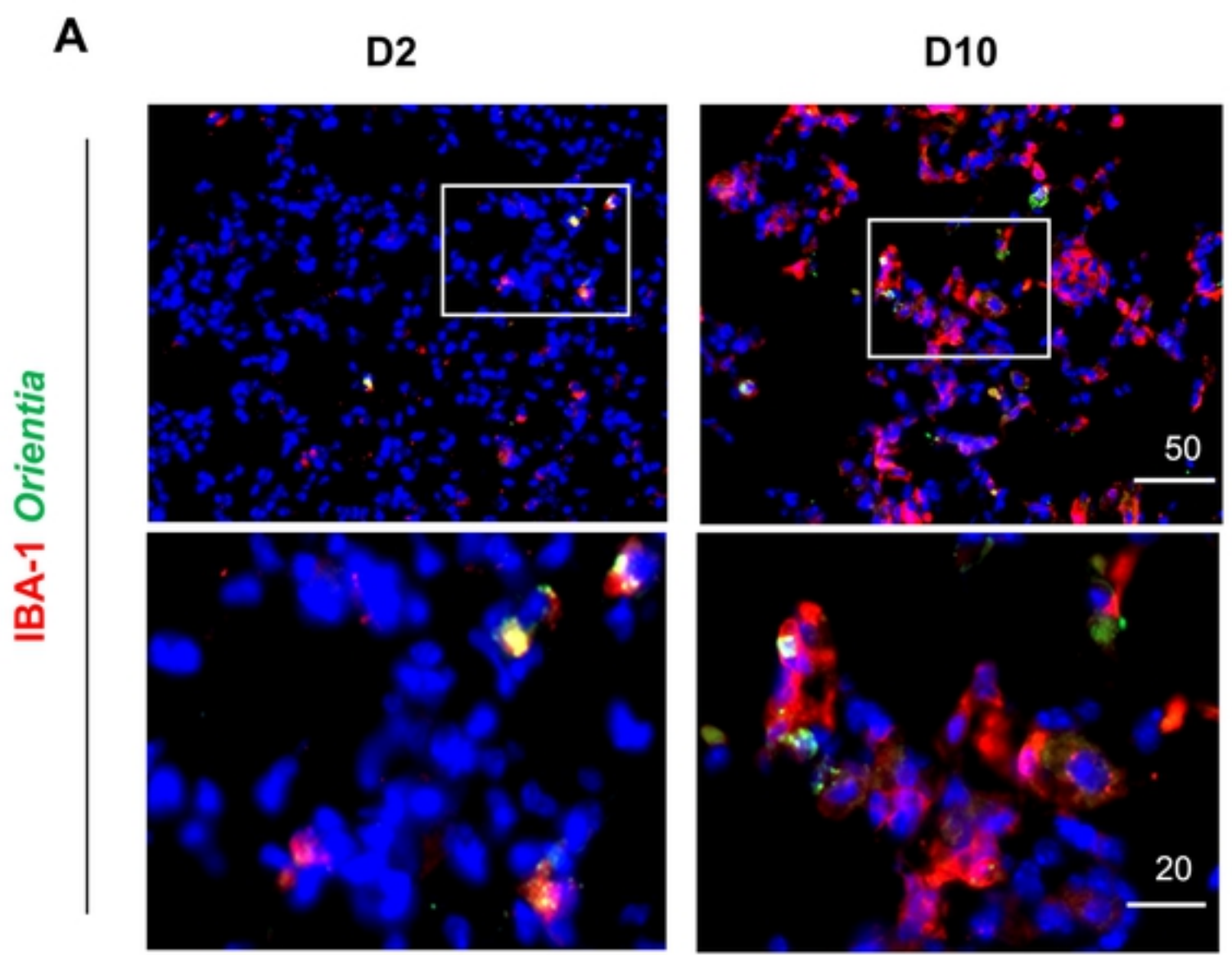


Figure S2



bioRxiv preprint doi: <https://doi.org/10.1101/723387>; this version posted August 2, 2019. The copyright holder for this preprint (which was not certified by peer review) is the author/funder, who has granted bioRxiv a license to display the preprint in perpetuity. It is made available under aCC-BY 4.0 International license.

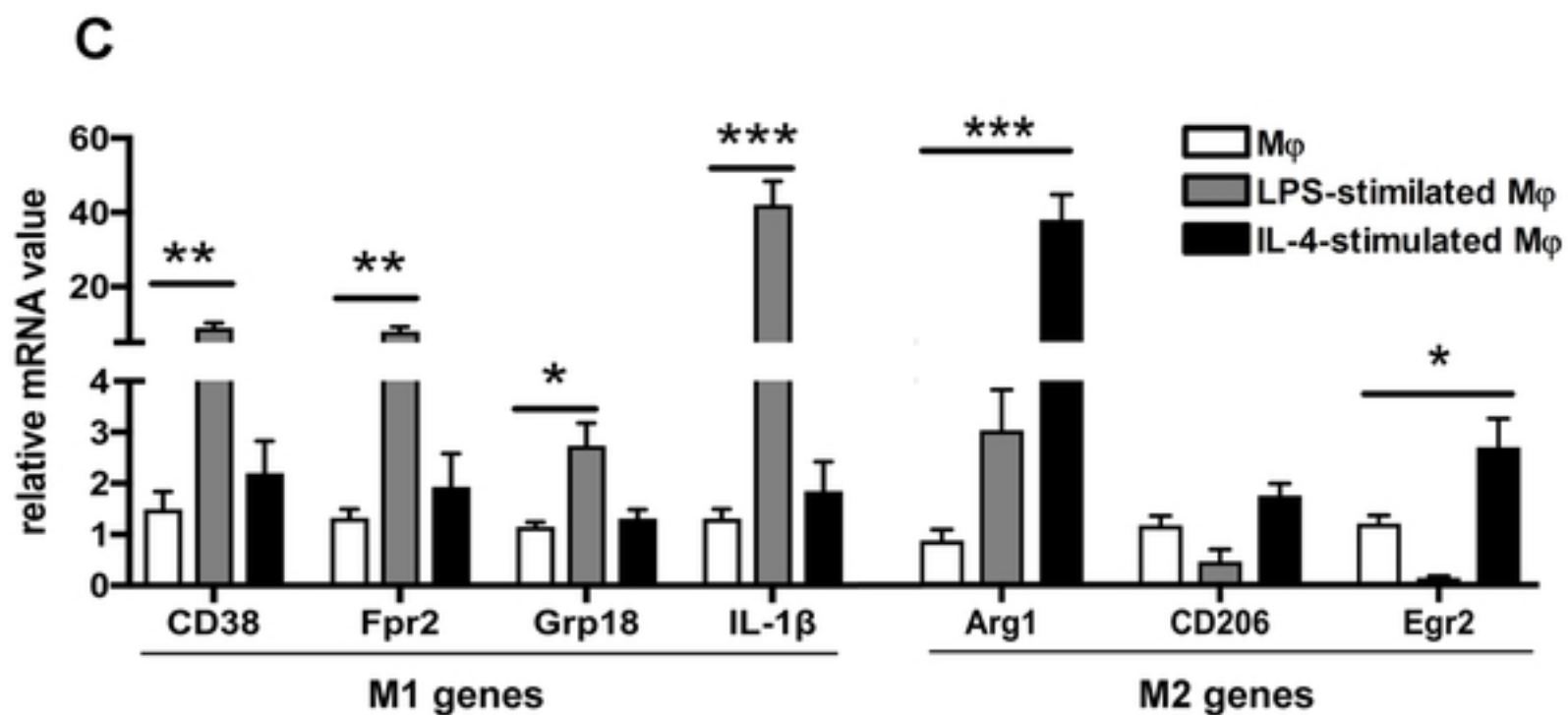
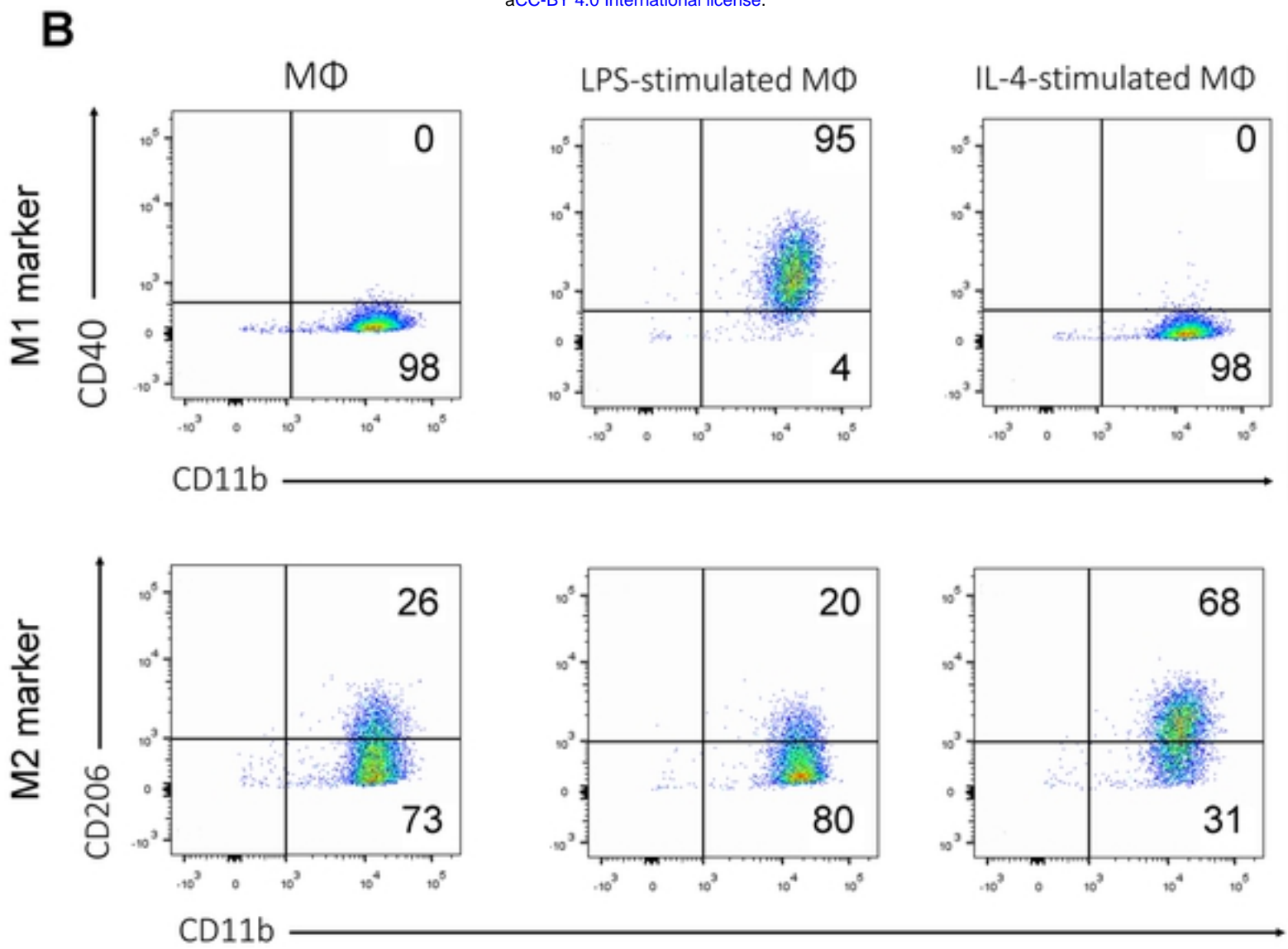


Figure S3